BWR Vessel and Internals Project Evaluation of Crack Growth in BWR Nickel Base Austenitic Alloys in RPV Internals (BWRVIP-59NP)

REPORT SUMMARY

The Boiling Water Reactor Vessel and Internals Project (BWRVIP), formed in
June 1994, is an association of utilities focused exclusively on BWR vessel and
internals issues. This BWRVIP report provides a methodology for assessing crack
growth in BWR nickel base alloy shroud support structures and in other nickel
base alloy components.

Background

Events in 1993 and 1994 involving the core shroud confirmed that intergranular
stress corrosion cracking (IGSCC) is a significant issue for austenitic materials used
in BWR internals. Following the initial evidence of IGSCC, US BWR utilities
formed the BWRVIP in June 1994, to address integrity issues arising from service
related degradation of key BWR internals components.

Among the key BWR internals components are the core shroud support structure
which includes the shroud support plate, the access hole covers, the shroud support
legs and/or gussets and vessel attachment brackets. These components are fabricated
from nickel base wrought materials and weld metal. Although limited cracking has
been observed to date in these materials in BWR internals, difficulty in inspection of
many of these internals components requires that the crack growth rates of these
materials for the key shroud support locations be determined. Without this information,
premature shroud support reinspection may be required, imposing an unnecessary
economic hardship on utilities.

Objectives

To formalize the methodology for determination of through-thickness IGSCC
growth rates in nickel base alloys based upon empirical field and laboratory test data
and field in-service inspection information.

Approach

The approach used was to determine through thickness residual stress and stress
intensity distributions for core support structure welds representative of the BWR
fleet. Both experimental and analytical techniques were used to determine the
residual stress distributions with reasonable agreement obtained. These residual
stresses were used in a fracture mechanics analysis to determine weld specific
through wall stress intensity distributions for welds H8, H9, H10, H11, and H12.
Crack growth distribution curves obtained from field and laboratory data and the

stress intensity factor distributions were used to perform crack growth evaluations for the individual welds.

Results

Crack growth rate disposition curves were developed for normal water chemistry (NWC) and hydrogen water chemistry (HWC) environments using Alloy 182 field and laboratory crack growth data.

Content Deleted -
EPRI Proprietary Information

EPRI Perspective

The correlations developed in this study can be used to conservatively predict the through thickness IGSCC growth of nickel base materials in the BWR environment in core support structure components. The residual stress distributions developed for a BWR-5, 6 design are believed to be generic to other BWR designs and can be used to disposition IGSCC in those welds. Application of this methodology provides assurance that BWRs with IGSCC in their nickel base welds can continue to operate safely while reducing utility costs by establishing reasonable inspection or reinspection intervals for these welds.

TR-108710NP

Interest Categories

Piping, Reactor, Vessel and Materials
Licensing and Safety Assessment

Key Words

Boiling Water Reactor
Core Shroud Support
Crack Growth Rate
Residual Stresses
Stress Corrosion Cracking
Nickel Base Alloys

BWR Vessel and Internals Project

Evaluation of Crack Growth in BWR Nickel Base Austenitic Alloys in RPV Internals (BWRVIP-59NP)

Prepared by:

Structural Integrity Associates
6615 Almaden Expressway, Suite 24
San Jose, CA 95118-1557

in Collaboration with

General Electric Nuclear Energy
Modeling & Computing Services
Entergy Operations, Inc.
EPRI Repair and Replacement Center
Berkeley Research and Engineering
Dominion Engineering, Inc.

Prepared for

BOILING WATER REACTOR VESSEL & INTERNALS PROJECT and

EPRI

3412 Hillview Ave.
Palo Alto, California 94304

DISCLAIMER OF WARRANTIES AND LIMITATION OF LIABILITIES

ORDERING INFORMATION

Acknowledgments

Executive Summary

The purpose of this report is to provide a methodology for assessment of crack growth in BWR nickel base austenitic alloy shroud support structure materials and welds, including attachments to the reactor pressure vessel made from these alloys. This work is applicable to components of Alloy 82, 182, and 600 types of nickel base austenitic materials. This methodology has been developed specifically for crack growth in the through-thickness direction. Residual and applied stresses and stress intensity factors have been developed for crack propagation in this orientation.

The steps involved in the development of the methodology include determination of residual stresses, stress intensity factors and crack growth rates based on an extensive database. The methodology involves development of crack growth disposition curves which can account for the variability of important intergranular stress corrosion cracking (IGSCC) parameters in providing a conservative, yet realistic assessment of the crack growth rate (CGR) in BWR nickel base austenitic alloys.

In Section 2 of this report, various core support structure configurations that are encountered in the BWR industry are discussed. The materials used in the design of the various configurations are presented. Most of the components are fabricated using Alloy 600 with welding performed using Alloy 82 and/or Alloy 182. The residual stress calculations done for this report used the specific geometry for a BWR-6 RPV fabricated by CBI Nuclear Company (CBIN). This geometry was chosen for the analyses because samples from an unused vessel were available for experimental stress analysis. The CBIN support structure design includes a number of weld configurations that are distinctly different from the geometries previously evaluated for BWR shrouds (Ref.: BWRVIP-14). These geometries include welds at the ends of support legs that are long slender beams (H10, H11, and H12), a weld between the annular shroud support plate and the OD of the shroud support cylinder (H8), and a weld between the shroud support plate and the ID of the cylindrical pressure vessel (H9). These welds are present with minor differences in component dimensions in vessels fabricated by CBIN for all BWR models. Vessels fabricated by Babcock and Wilcox (B&W) use a similar leg design for the shroud support, though with thinner

material for the legs. The results of the analyses in this report are considered to be representative of the stress and stress intensity distributions for corresponding weld geometries in all CBIN and B&W fabricated vessels when scaled to the correct component thicknesses (i.e., dimensions for distributions are normalized by the component thickness). Vessels fabricated by Combustion Engineering (CE) used an annular shroud support plate reinforced by gusset plates shroud support design. This design includes an H9 weld similar to the one analyzed for this report. Weld H8 for the CE shroud support design is between the end of the shroud support cylinder and the top surface of the shroud support plate. This configuration is similar to shroud welds H3, and H6a. Thus, the results of shroud weld evaluations (Ref.: BWRVIP-14) can be used to evaluate the H8 weld in the CE design shroud support.

Also in Section 2, the performance of the core support structural materials and welds relative to IGSCC is discussed. In general, the performance of Alloys 600, 82 and 182 have been relatively good in the absence of a crevice condition or weld defects. This is borne out by field experience which has shown that these components have not exhibited significant cracking when compared to austenitic stainless steel components. However, under creviced condition, these alloys can become highly susceptible to IGSCC. These materials have a very long crack initiation phase which contributes to their relatively good performance.

In order to calculate the fracture mechanics stress intensity factor, the stresses in the core shroud support structure must be known. The operating stresses of the shroud support structure are relatively low and can be determined readily from the stress reports. A major portion of Section 3 of this report deals with weld residual stresses developed during the fabrication of the shroud and the shroud support structure. Both experimental measurements and analytical techniques were used to determine surface and through-wall residual stress distributions for the welds of the support structure.

In Section 4 of this report, established fracture mechanics models were used to determine the through-wall stress intensity factor (K) distributions for the through-wall stress profiles.

Individual stress distributions determined for each weld of the core support structure were used to develop the through-wall K distribution for each weld. For welds H8 and H9, the K distributions were determined for both a 360 flaw and for various finite length flaws. For the leg welds, H10, H11 and H12, the K distribution was derived assuming the flaw extends over the entire width of the leg.

In Section 5 of this report, an extensive database consisting of nickel base austenitic alloy crack growth rates is described. These data came from General Electric Nuclear Energy (GENE) and BWRVIP data generated through the peer review process and include both experimental data points and in-plant crack arrest verification system (CAVS) data. Most of the data in the database have adequate definition of environmental conditions and other important crack growth parameters thus permitting a more realistic generic crack growth model to be developed. The database has been used to derive crack growth disposition curves which account for environmental conditions such as conductivity of the water and the electrochemical potential (ECP).

In Section 6, evaluations using the crack growth dispositions curves and the derived through-wall stress intensity factor distributions were performed to determine the crack growth for all the welds under various water chemistry conditions.

Content Deleted - EPRI Proprietary Information

**Content Deleted -
EPRI Proprietary Information**

The BWRVIP proposes that the methodology presented in this report be used to evaluate crack growth in core support structure welds and other Alloy 82, 182 and 600 welded internal components.

Table of Contents

List of Tables

List of Figures

List of Figures (concluded)

1.0 INTRODUCTION

1.1 Background

The nickel based austenitic alloys, wrought alloy 600 and the weld metals alloy 82 and 182, have been used extensively in boiling water reactor (BWR) application where excellent material toughness, compatibility with vessel material properties and resistance to stress corrosion cracking (SCC) are required. Included in those structural applications are vessel internals components such as:

> access hole covers
>
> safe ends
>
> shroud head bolts
>
> shroud support structure
>
> vessel attachment brackets

Although the performance of these alloys has generally been excellent in these and other BWR structural applications, some modest incidents of intergranular stress corrosion cracking (IGSCC) have occurred. These cracking incidents, combined with laboratory data illustrating susceptibility of these alloys to IGSCC initiation and growth, have resulted in major research activities sponsored by the Electric Power Research Institute (EPRI), vendors and contractors such as General Electric Company (GE), research groups and the Nuclear Regulatory Commission (NRC) to understand and mitigate the cracking problem in these alloys.

The BWR Vessel and Internals Project (BWRVIP) has prepared a safety assessment of BWR internals [1] addressing issues requiring resolution affecting vessel internals components. Among the issues requiring resolution are the issues of crack growth rates among the various structural materials comprising the vessel internals. An earlier BWRVIP report developed IGSCC crack growth correlations for austenitic stainless steel as a function of water quality,

electrochemical potential (ECP) and stress or stress intensity [2]. The methodology utilized in the austenitic stainless steel activity was to determine the crack growth rate as a function of stress intensity for various water purity and ECP conditions, assess the state of applied and residual stress (including weld residual stress) on the core shroud by analytical and experimental methods and develop stress intensity models for which crack growth rates could be determined. Because of the differences in performance of nickel based alloys relative to stainless steel and the differences in the structural configurations for which these materials are used in the RPV internals, it is necessary to develop an independent crack growth model for application to nickel based alloys.

1.2   Susceptibility of Nickel Based Components in the BWR Environment

The objective of this report is to provide the methodology to disposition a flaw in a nickel based component in the BWR environment. To that end, the susceptibility of these materials to IGSCC must be provided. Of specific importance to a flaw disposition evaluation is the crack growth rate of the material. The susceptibility of these materials to crack initiation, while important to the overall reliability of these components, is not the specific charter of this document.

The materials of the shroud support structures are mainly nickel based alloys 600, 82, and 182. The performance of these alloys in BWR service has been quite good. In some instances, IGSCC has initiated in these materials where crevices or weld root defects have been observed. These locations include creviced thermal sleeve attachment to nozzle safe ends, a feedwater nozzle where a weld root defect initiated IGSCC and access hole covers (AHC) where partial penetration welding was sometimes performed. In these instances, the cracking has occurred predominately in Alloy 182, the nickel base flux-coated electrode used for welding these components. Some limited cracking has also been observed in the Alloy 182 welds where crevices or weld root defects were not obviously present. These incidences include cracking in a recirculation system outlet nozzle to safe end butter in a domestic BWR and in steam dryer

assembly attachment brackets in two foreign BWRs. In most instances where IGSCC has occurred, the cracking was limited in extent, involving multiple short cracks. Some were circumferential, such as in access hole covers and in nozzle to safe end welds. Some were axial, crossing a weld bead as observed in nozzle to safe end welds. In most documented cases of IGSCC in the BWR, the cracking initiated in the Alloy 182 weld metal, propagating in some instances into the Alloy 600 wrought material or progressing slightly into the low alloy steel nozzle to which the Alloy 182 was welded.

The mechanism for IGSCC in nickel based alloys in the BWR environment appears to be similar to that for austenitic stainless steel. The generally accepted factors responsible for IGSCC of these alloys are sufficient tensile stress, thermal sensitization and a sufficiently oxidizing environment. As in the case of austenitic stainless steels, additional aggravating factors include the presence of crevices.

The following paragraphs describe briefly the susceptibility of each of the nickel base alloys to IGSCC initiation and propagation. More details of the susceptibility of these alloys to IGSCC in the BWR environment are provided in References 3, 4 and 5.

Alloy 600

Alloy 600 has been used extensively as the structural material of the shroud support in the BWR. The IGSCC performance of Alloy 600 in the absence of crevices has been excellent. Recent in-reactor and laboratory testing sponsored by EPRI [3] has confirmed the high IGSCC initiation resistance of this alloy.

Content Deleted - EPRI Proprietary Information

**Content Deleted -
EPRI Proprietary Information**

Alloy 182

Alloy 182 is typically utilized within the reactor pressure vessel for limited vessel cladding application, vessel attachment pad buildups, the shroud support plate to vessel pad weld, the shroud support gusset welds, the shroud support leg welds, the shroud support to shroud weld and the access hole cover to shroud support plate weld.

Recent in-reactor and laboratory testing has confirmed the IGSCC crack growth can occur in Alloy 182 material in the BWR environment [3].

**Content Deleted -
EPRI Proprietary Information**

Alloy 82

Alloy 82 is a bare filler wire which is used in BWRs where very high quality gas tungsten arc-welding (GTAW) is employed. It has been widely used as a welding insert for butt welds, and is used for the root and hot passes of many structural welds. This alloy is higher in chromium and lower in carbon than Alloy 182 and, therefore, has improved resistance to IGSCC initiation and growth in the BWR environment compared to Alloy 182. EPRI-sponsored testing has verified the excellent resistance of this alloy to IGSCC, and the NRC has identified this material as an IGSCC resistant alloy in NUREG-0313, Revision 2 [6]. In the HWC environment, the IGSCC resistance of Alloy 82 is further enhanced.

1.3   BWR Plant Operating Experience

The operating experience with nickel based alloys in the BWR environment has been excellent, provided no design or metallurgical crevice is present (such as a weld defect). A total of 34 domestic BWRs have had either visual or UT inspection performed of their nickel based wrought materials and weld metal [8].

In summary, the performance of Alloy 182 and the other nickel based alloys used as structural materials in the BWR has been good, when crevices or weld root defects are absent. Crack initiation in uncreviced components has been limited in extent in these materials as noted above. Where crack initiation has occurred, the crack extension on the surface appears to have been limited, consistent with the observation that crack initiation is difficult in these materials. This observation has also been confirmed by laboratory testing which has demonstrated the difficulty in initiating IGSCC in nickel based alloys in simulated BWR environments where crevices or weld root defects are absent.

1.3.1 Surface Crack Growth Rates of Nickel Base Alloys

As highlighted above, only limited crack initiation has been observed in non-creviced nickel base alloys in BWR service. The three plants having reported indications noted that the extent of surface cracking was limited. In each case, the defects were allowed to remain during one or more additional operating cycles. Little or no surface crack extension was observed in the plants where the cracking had been observed. In the foreign plant, the indications were observed for three years before removal. In one of the domestic BWRs, the indications are still being monitored. The cracked component was removed and rewelded in the other domestic BWR.

The field observations support several conclusions.

1.4   Objectives and Approach

The objective of this report is to formalize the methodology for determination of nickel base austenitic alloy crack growth rates, based on empirical data that account for parameters that are known to affect crack propagation in the BWR. These crack growth rates (CGR) will then be available for use in the evaluation, inspection and repair criteria for BWR RPV internal components. The scope of CGR influencing factors will be tied to material susceptibility, water environment, and stress-state parameters associated with the core support structure welds. A model is presented that incorporates the effects of the important factors into a conservative, yet realistic, crack growth disposition curves for nickel based alloys in the BWR internals. The model developed in this report is developed for through-thickness crack growth based upon available test data and is based upon analysis of available test data. The model has been formulated with material, environment, and stress data which result from laboratory and in-plant test programs. It is then tested against field data and found to provide realistic upper bound estimates of growth rates observed over the BWR operating regime.

Although several different structural configurations for the core support structure have been used in BWRs, the present study focuses on the structural configuration of a BWR-6 because it is believed that this configuration can be used to bound the BWR-3 and 4s. Other work done by the BWRVIP on the core shroud and the reactor pressure vessel addresses the welds of the other core shroud support structures. The motivation for choosing a BWR-6 design for this study lies in the fact that components from two plants of that design (River Bend Nuclear Station and Grand Gulf Nuclear Station) were readily available for experimental measurements of residual stresses. The analytical studies used in this report were benchmarked against the experimental residual stress measurements and once benchmarked and found to be valid, can be used generically. The present study focuses on five welds of a BWR-6. These are welds H8, H9, H10, H11 and H12. Experimental measurements were performed only on welds H8, H9, H10 and H12 since no weld exists for the H11 location at River Bend or at Grand Gulf. However the analytical evaluations are also extended to Weld H11.

The following sections of this report describe the work undertaken within this project to understand the state of stress, and material variability on the crack growth rates of nickel base alloys in the core shroud support structure. Section 2 provides a description of the various core shroud support structure designs in the BWR industry and the materials used in the fabrication of the structure. The IGSCC susceptibility of these materials and their field performance is also discussed in this section. Section 3 provides the operating and residual stress data for the core support structure welds. Fracture mechanics methods employed in determining the stress intensity factors associated with the applied and residual stresses are presented in Section 4. Section 5 presents a compilation and assessment of crack growth data produced by laboratories and in field testing. This collection of data provides a compiled database for use in determining crack growth rates as a function of environment and stress intensity in nickel base austenitic alloys. This section also provides crack growth rate disposition curves developed using material, environment and stress information. Section 6 presents crack growth evaluation methodology for estimation of crack growth rates in the through-thickness direction for BWR shroud support structure welds.

2.0   BWR SHROUD SUPPORT WELD CONFIGURATIONS

The shroud support structures for most BWRs are defined as those structural regions below the H7 weld in the core shroud (Figure 2-1). The shroud support consists generally of the support plate and cylinder and generally includes either gussets or legs. The shroud support structure is typically fabricated from Alloy 600 although in some plants Type 304 stainless steel was used. For all nickel alloy welds, the weld metal used was either Alloy 82 or 182.

The purpose for the shroud support is to provide support for the core plate, jet pumps, core shroud, top guide, core spray spargers and annulus piping and the shroud head/steam separator dryer assembly. The shroud support also supports the weight of peripheral fuel bundles, and provides lateral restraint to the fuel during seismic or other dynamic events. The shroud support also forms part of the core coolant envelope in the event of a recirculation system line break (loss of coolant accident).

There are several shroud support designs, varying from one BWR model to another and even within a BWR model design. The basic four designs are identified as follows:

> Conical Shroud Support Plate (BWR-2)
> Thick Shroud Support Plate (Hatch Unit 2)
> Shroud Support Plate with Legs
> Shroud Support Plate with Gussets

Detailed descriptions of these designs are provided in Reference 9. For completeness, abbreviated descriptions from the Reference 9 report are repeated in the following sections.

2.1   Conical Shroud Support Plate (BWR-2)

The shroud support in the two operating U. S. BWR-2 plants (Nine Mile Point Unit 1 and Oyster Creek) is a 1.5 inch thick conical design fabricated by Combustion Engineering (CE). This configuration is shown in Figure 2-2.

Content Deleted -
EPRI Proprietary Information

2.2   Thick Shroud Support Plate (Hatch Unit 2)

The shroud support design in the Hatch Unit 2 plant (BWR-4) is an 8.8 inch thick flat plate design fabricated by CE. This configuration is shown in Figure 2-3.

Content Deleted -
EPRI Proprietary Information

2.3   Shroud Support Plate with Legs

The shroud support design implemented at the majority of the BWR-3, 4, 5 and 6 plants, in particular the Babcock & Wilcox (B&W) and Chicago Bridge & Iron Nuclear (CBIN) constructed RPVs, is a flat plate design with support legs that connect to the RPV bottom head. At some plants, an Alloy 600 stub tube is welded to an attachment pad on the inside of the RPV

lower head, and the leg is welded to the top of the stub and to the bottom face of the shroud support cylinder (Figure 2-4). At other plants, the legs are welded directly to the attachment pad on the inside surface of the RPV lower head (Figure 2-5). At some plants, the legs are reinforced with stiffeners, which run vertically and are welded to the middle of the inner and outer (radial) surfaces of each leg (Figure 2-5).

**Content Deleted -
EPRI Proprietary Information**

2.4   Shroud Support Plate with Gussets

The shroud support design used at a number of BWR-3, 4 and 5 plants, the CE-fabricated plants, is a cantilevered plate design with twenty-two support gussets, rather than support legs, that connect to the RPV wall. The gussets vary in size and thickness among plants, and are fabricated from Alloy 600 material. The welds of interest are the welds attaching the gusset to the support plate and the gusset to the vessel. This is shown in Figure 2-6.

**Content Deleted -
EPRI Proprietary Information**

2.5 Shroud Support Structure Used in this Study and Applicability to Other Shroud Support Structures

The study described in this report was conducted on a BWR-6 design. The choice of a BWR-6 for this study is motivated in part by the fact that the spare vessel at River Bend, a BWR-6 was available to be used for experimental residual stress measurements to supplement the analytical evaluation to be presented in this report. It is believed, however, that with the exception of the BWR-2 design shown in Figure 2-2 (limited to only Nine Mile Point Unit 1 and Oyster Creek), the present study and results of other work performed by the BWRVIP for the core shroud [2] and the reactor vessel attachment welds [10] can be used to address the welds of all the remaining core shroud support structure configurations shown in Figures 2-3 through 2-6.

**Content Deleted -
EPRI Proprietary Information**

The dimensions of the River Bend Support Structure are shown in Figure 2-7. The experiment study will focus on welds H8, H9, H10 and H12 since weld H11 is not present in the core support structure at River Bend. However, weld H11 will be addressed as part of the analytical effort. In order to provide details of these welds for the analytical studies, photomacrographs of

these welds were taken so that the details could be included in the modeling process. The photomacrograph are shown in Figures 2-8 through 2-11 for the four welds considered in the experimental study.

H3

H4

H5

H6a/H6b

H7

H8 ——— ●———— H9

H10

H11

H12

Reactor Pressure Vessel

Core Shroud

Shroud Support Cylinder
Shroud Support Plate

Core Shroud Support Leg

98068r0
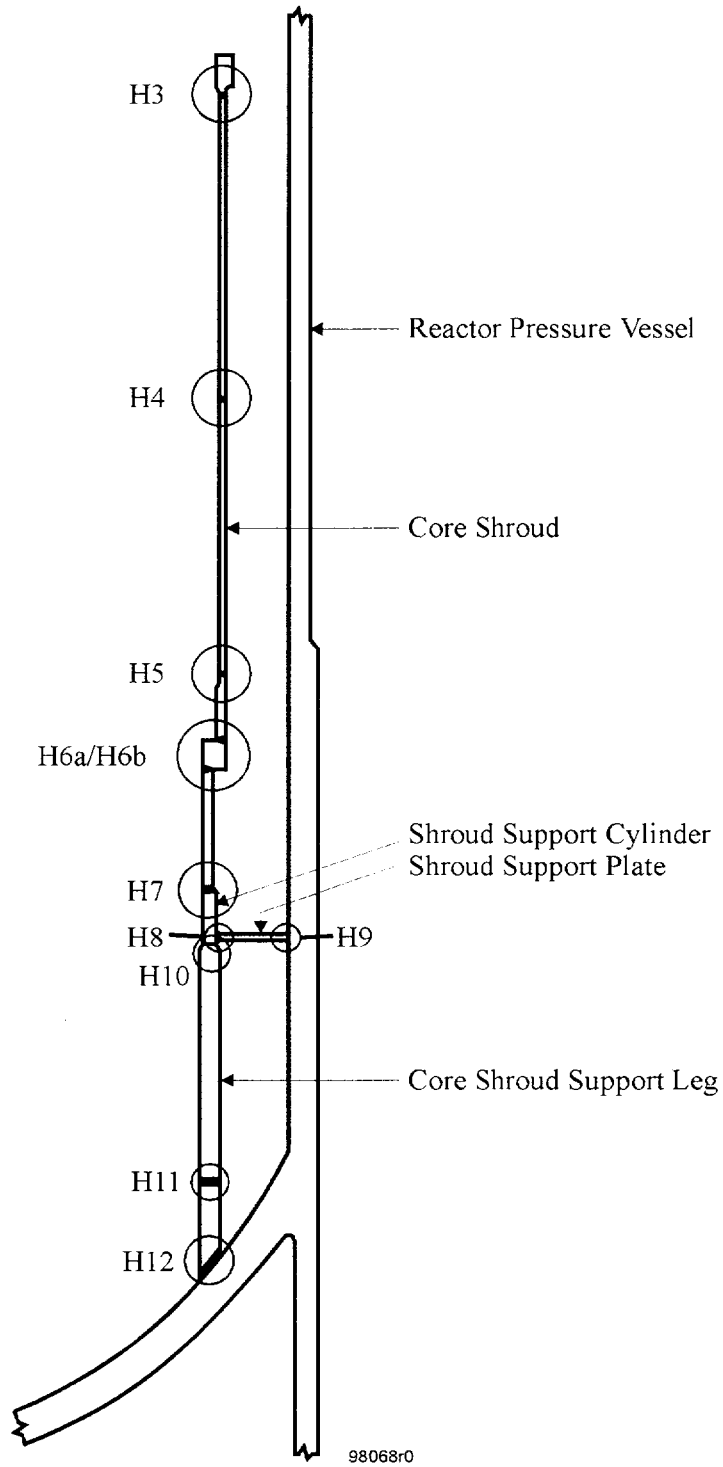
Figure 2-1. Typical Arrangement of Core Shroud and Support Structure (BWR-6)

**Content Deleted -
EPRI Proprietary Information**

Figure 2-2. BWR-2 Shroud Support Configuration

**Content Deleted -
EPRI Proprietary Information**

Figure 2-3. Hatch Unit 2 Shroud Support Configuration

**Content Deleted -
EPRI Proprietary Information**

Figure 2-4. Shroud Support Plate With Legs (CBIN BWR-4, 5, 6 Design)

**Content Deleted -
EPRI Proprietary Information**

Figure 2-5. Shroud Support Plate With Legs (B&W BWR-3, 4 Design)

**Content Deleted -
EPRI Proprietary Information**

Figure 2-6. Shroud Support Plate With Gussets Configuration (CE BWR-3, 4, and 5 Design)

**Content Deleted -
EPRI Proprietary Information**

Figure 2-7. Geometry and Dimensions of the Core Support Structure at River Bend

**Content Deleted -
EPRI Proprietary Information**

Figure 2-8. Photomacrograph of Weld H8 at River Bend

**Content Deleted -
EPRI Proprietary Information**

Figure 2-9. Photomacrograph of Weld H9 at River Bend

**Content Deleted -
EPRI Proprietary Information**

Figure 2-10. Photomacrograph of Weld H10 at River Bend

**Content Deleted -
EPRI Proprietary Information**

Figure 2-11. Photomacrograph of Weld H12 at River Bend

3.0 OPERATING AND RESIDUAL STRESSES

Stresses in the core shroud support welds can be divided into two broad categories. The first category is associated with loads with various plant operating conditions. The second is associated with fabrication stresses which arise when the component are welded together. Major contributors to the fabrication stresses are the weld residual stresses caused by the thermo-plastic strains associated with the welding and the locked-in or fit-up stresses due to restraint of various parts of the structure during fabrication.

3.1 Operational Stresses

A detailed description of the operational loads acting on the shroud support structure and the load combinations for the various service levels can be found in the vessel stress reports for the plants. The primary loads consist of pressure, deadweight, buoyancy, seismic and hydrodynamic loads. Secondary stresses result from loadings associated with thermal and pressure expansion of the RPV.

Content Deleted - EPRI Proprietary Information

3.2 Weld Residual Stresses

Unlike piping butt welds in which the residual stresses are essentially independent of the fabrication sequence due to the flexibility in the system, the residual stresses in the shroud support structure are affected very significantly by the fabrication process. This is because the support structure arrangement produces a very highly constrained structure and the manner in which the structure is restrained during the welding process plays a key role in determining the

final state of the residual stresses. For the River Bend vessel which was considered in this evaluation, the weld sequence used was based on procedures used by Chicago Bridge and Iron (CBI), the fabricator of the vessel.

**Content Deleted -
EPRI Proprietary Information**

In addition to the fabrication sequence, other factors that affect the residual stresses in the support structure welds include heat input during the welding process, welding sequence for each particular weld, weld starts and stops, cooling time between phases, base/weld metal mechanical properties, local weld repairs and post weld heat treatment.

**Content Deleted -
EPRI Proprietary Information**

Both experimental and analytical studies were performed to determine the magnitude and distribution of the weld residual stresses in the River Bend support structure. The purpose of determining the residual stresses using both methods is to use the experimental measurements to benchmark the analytical study such that the analytical approach can be used with confidence to determine the residual stresses associated with other shroud support structure configurations discussed in Section 2 of this report without the need for additional experimental measurements.

3.2.1   Through-Thickness Residual Stress Measurements at River Bend Nuclear Station

Through-wall residual stress measurements of the shroud support structure welds H8, H9, H10 and H12 at River Bend were performed by University of California, Berkeley personnel using the crack compliance method (Appendix B). Specimens containing all the four welds were cut out from coupons removed from the core shroud support structure and the vessel. Photomacrographs of the welds are presented in Figure 2-8 through 2-11. The cutting process of the coupons from the support structure is provided in Reference 11. As discussed earlier, it is expected that the residual stresses are influenced by the forces and moment developed in the constrained structure during fabrication. Cutting out of the specimens from the support structure released the part of the residual stresses associated with the constraint of the structure. Hence the measurements of the residual stresses presented herein only account for that part of the local residual stress associated with the thermo-plastic strains during the welding that are locally balanced with no resultant external loads.

The theoretical background of the crack compliance method and details of the methodology in application to the measurements of the shroud at River Bend are provided in Appendix B of this report. In summary, the method involves installing a strain gage at an optimal location of a specimen containing the weld.

**Content Deleted -
EPRI Proprietary Information**

**Content Deleted -
EPRI Proprietary Information**

The above procedure was used to determine the through-wall residual stress distribution in the shroud for welds H8, H9, H10 and H12. The geometry of the specimens that were used to obtain the measurements and the weld profiles as well as location of the measurements are shown in Figures 3-1 through 3-4. The strain and the through-wall residual stress distributions are presented in Appendix B of this report.

3.2.2 Analytical Determination of Residual Stresses

In addition to the experimental determination of the weld residual stress for the various welds of the shroud support structure at River Bend, finite element analyses were performed by Dominion Engineering Inc. to analytically determine the weld residual stresses. The objective of performing analytical and experimental studies on equivalent welds was to allow the analytical results to be benchmarked against experimental results for actual BWR components. Because of the fact that experimental measurements were made on samples that represent only a small fraction of the total weld and the simplifying assumptions that must be used to make analysis tractable, exact agreement between the analytical and experimental results is not expected. However, the experimental and analytical results are generally in agreement with regard to the magnitudes of peak stresses and the shapes of the through thickness variations in stress. This reasonable agreement provides a basis for using analysis to determine residual stress distributions for other shroud support structure configurations for which experimental results are unavailable.

The analyses were performed using the geometrical data of the core support structure configuration at River Bend in order to provide consistent and comparable results with the experimental stress measurements performed at River Bend.

**Content Deleted -
EPRI Proprietary Information**

**Content Deleted -
EPRI Proprietary Information**

Details of the analyses and the analyses results for all the welds in the core shroud support structure are presented in Appendix D of this report. The results are presented in terms of contour plots as well as through-wall distribution of hoop and axial stresses at key locations of the weldments including the locations where the experimental measurements were taken to provide the basis for comparison. Since the analysis results indicate that there is variation of stresses along the leg of the support structure, the through-wall stress distribution are presented for several discrete locations along the leg. This is even more so for the H8 and H9 welds because in addition to the discrete legs, the jet pump and the access hole cover holes interact with the H8 and H9 welds. Results of the through-wall stress distributions for welds H8, H9, H10 and H12 for the as-welded as well as the stress relieved conditions are presented in Appendix D of this report. The following presents the summary of the observation made on the analytical results detailed in Appendix D.

Content Deleted - EPRI Proprietary Information

**Content Deleted -
EPRI Proprietary Information**

3.2.3 Comparison of Calculated and Measured Residual Stresses

The through-wall residual stress measurements reported earlier are compared with the analytical predictions for all the welds (with the exception of H11) with the purpose of establishing consistency between experiment and analysis, and to provide a recommendation for appropriate distributions which should be used in crack growth evaluation. The comparison is made by considering the trends and peak magnitudes rather than point by point numerical comparisons because, as discussed earlier, the final state of residual stress in each weld or portion of weld is affected significantly by the degree of constraint imposed by the remainder of the structure during fabrication and this is likely to be different from plant to plant and from point to point on the weld. It is also recognized that there are several designs of shroud support structures as discussed in Section 2 of this report and residual stress measurements for all is not possible. Hence, if the analytical predictions are supported by the measured values, it will provide a basis for using only analytical means to determine the residual stresses in the future for other core shroud support structure configurations.

The comparisons of the calculated and measured residual stresses are presented in Figures 3-5 to 3-8.

**Content Deleted -
EPRI Proprietary Information**

**Content Deleted -
EPRI Proprietary Information**

The reasonable agreement between measured data and adjusted analytical results indicates that the analytical approach used for the calculations gives a satisfactory simulation of the welding process with respect to generation of residual stresses. Thus, analysis can be used to obtain reasonable estimates of weld residual stress distributions in other shroud support structure configurations where no experimental data are available.

**Content Deleted -
EPRI Proprietary Information**

Content Deleted -
EPRI Proprietary Information

3.2.4 Stress Relaxation During Crack Growth

Because of the constraint in the structure resulting in locked-in forces and moments, it is
expected that the locked-in stresses will be relaxed when an assumed crack propagates through
the thickness. In order to determine the relaxed stresses as a crack propagates through the
thickness, a series of analyses were performed in Appendix D in which a line of elements
through the weld (representing the crack) were successively "killed" and after each kill the stress
path data was recalculated. This was performed for both the as-welded condition and post-
welded heat treated conditions for weld H8 and H9 and presented in Appendix D.

Table 3-1

Strain Measurement for Grand Gulf Support Legs

**Content Deleted -
EPRI Proprietary Information**

**Content Deleted -
EPRI Proprietary Information**

Figure 3-1. Through-Thickness Measured Residual Stress Distribution (σ_x) for Weld H8

**Content Deleted -
EPRI Proprietary Information**

Figure 3-2. Through-Thickness Measured Residual Stress Distribution ($_x$) for Weld H9

**Content Deleted -
EPRI Proprietary Information**

Figure 3-3. Through-Thickness Measured Residual Stress Distribution ($_x$) for Weld H10

**Content Deleted -
EPRI Proprietary Information**

Figure 3-4. Through-Thickness Measured Residual Stress Distribution ($_x$) for Weld H12

**Content Deleted -
EPRI Proprietary Information**

Figure 3-5. Comparison of Analytical with Measured Residual Stress for Weld H-8

**Content Deleted -
EPRI Proprietary Information**

Figure 3-6. Comparison of Analytical with Measured Residual Stress for Weld H-9

**Content Deleted -
EPRI Proprietary Information**

Figure 3-7. Comparison of Analytical with Measured Residual Stress for Weld H10

**Content Deleted -
EPRI Proprietary Information**

Figure 3-8. Comparison of Analytical with Measured Residual Stress for Weld H12

**Content Deleted -
EPRI Proprietary Information**

Figure 3-9. Strain Gage and Cut Locations During Measurement at Grand Gulf

**Content Deleted -
EPRI Proprietary Information**

Figure 3-10. Deflection (Towards Vessel Wall) of Support Leg After Cutting

**Content Deleted -
EPRI Proprietary Information**

Figure 3-11. Change in Axial Strain in the Support Legs at Grand Gulf After Cutting

**Content Deleted -
EPRI Proprietary Information**

Figure 3-12. Change in Transverse Strains in the Support Legs at Grand Gulf After Cutting

4.0   FRACTURE MECHANICS CONSIDERATIONS

The fracture mechanics parameter which is key in the crack growth evaluation of components is the stress intensity factor (K_1). In this section, the derivation of the stress intensity factor for all the core shroud support structure welds is discussed. Separate fracture mechanics models are used to determine the K_1 distribution for the completely 360 weld configuration cracks (H8 and H9) and for the leg welds with finite length cracks (H10, H11 and H12).

4.1   Stress Intensity Factor for Welds H8 and H9

Welds H8 and H9 extend around the entire circumference of the shroud and RPV respectively. Because the possibility of a crack extending completely around the circumference is very unlikely, finite length flaws were considered in the derivation of K_1 for these components.

**Content Deleted -
EPRI Proprietary Information**

**Content Deleted -
EPRI Proprietary Information**

**Content Deleted -
EPRI Proprietary Information**

The results of the K_I determination for welds H8 and H9 as shown in Figure 4-1 through 4-4 for various aspect ratios for the as-welded condition. K_I distributions are shown for both the FEA presented in Section 3 since this case represents the actual stress condition for these welds. For each case, K_I is shown for crack growing from top-to-bottom as well as bottom-to-top.

**Content Deleted -
EPRI Proprietary Information**

4.2   Stress Intensity Factor Determination for Welds H10, H11 and H12

Welds H10, H11 and H12 are considered separately since they are leg welds and as such, they have a finite width. When a section of the support leg is parted out, the change in stresses is mainly caused by releasing the locked-in force and the moment. The change in stress due to the parting out can be estimated if the deformation associated with the parting out is available. If the deformation due to parting-out is unavailable, it is necessary to estimate the change in stresses from the boundary condition and welding sequence.

For welds H10 and H12 located respectively on the top and bottom of the support leg, the resultant moment, which is locked in after weld H10 is made, consists of two parts:

Content Deleted -
EPRI Proprietary Information

**Content Deleted -
EPRI Proprietary Information**

**Content Deleted -
EPRI Proprietary Information**

For weld H10, the as-welded and the post-weld-heat-treated (PWHT) stress distributions are shown in Figures 4-7 and 4-8 respectively. The corresponding stress intensity factors are obtained and shown in Figure 4-9.

**Content Deleted -
EPRI Proprietary Information**

For weld H12, the as-welded stress distribution is shown in Figure 4-10. The corresponding stress intensity factors are obtained and shown in Figure 4-11. Similarly the as-welded stress distribution and the corresponding K distribution for weld H-11 are shown in Figures 4-12 and 4-13, respectively.

**Content Deleted -
EPRI Proprietary Information**

Figure 4-1. K_I Distribution for Weld H8 in As-Welded Condition (FEA - Top-to-Bottom)

**Content Deleted -
EPRI Proprietary Information**

Figure 4-2. K_I Distribution for Weld H8 in As-Welded Condition (FEA - Bottom-to-Top)

**Content Deleted -
EPRI Proprietary Information**

Figure 4-3. K_I Distribution for Weld H9 in As-Welded Condition (FEA - Top-to-Bottom)

**Content Deleted -
EPRI Proprietary Information**

Figure 4-4. K_I Distribution for Weld H9 in As-Welded Condition (FEA - Bottom to Top)

**Content Deleted -
EPRI Proprietary Information**

Figure 4-5. Bending Deformation Associated with the Restraint at the Top of the Leg

**Content Deleted -
EPRI Proprietary Information**

Figure 4-6. An Edge-Cracked Beam with Non-Uniform Thickness and Fixed Ends

**Content Deleted -
EPRI Proprietary Information**

Figure 4-7. Residual Stress in Weld H10 in As-Welded Condition

**Content Deleted -
EPRI Proprietary Information**

Figure 4-8. Residual Stress in Weld H10 After Stress Relief

**Content Deleted -
EPRI Proprietary Information**

Figure 4-9. Normalized K_I Computed for Weld H10

**Content Deleted -
EPRI Proprietary Information**

Figure 4-10. Residual Stress in Weld H12 in As-Welded Condition

**Content Deleted -
EPRI Proprietary Information**

Figure 4-11. Normalized K_I for Weld H12 in As-Welded Condition

**Content Deleted -
EPRI Proprietary Information**

Figure 4-12. Residual Stress Distributions for Weld H11

**Content Deleted -
EPRI Proprietary Information**

Figure 4-13. Normalized K_I for Weld H11

5.0 CRACK GROWTH DISPOSITION CURVES

Beginning in the 1970s and continuing to the present, General Electric Nuclear Energy (GENE) has performed studies of the behavior of Alloy 182 and Alloy 600 structural materials that are used throughout the BWR. These studies have included laboratory stress corrosion tests, crack initiation tests, crack growth tests involving the measurement of crack growth rates in the laboratory and in reactor site testing systems. GENE has also evaluated field cracking and performed failure analyses. GENE has provided IGSCC updates to the NRC on a regular basis to aid in the dissemination of data and understanding of the technical issues. Over the past 15 years, GENE has accumulated data bases on field behavior of these materials and has continually been involved with evaluating plant cracking.

Using this historical foundation coupled with current understanding about SCC, disposition crack growth rate curves for use with Alloy 182 weld metal and Alloy 600 can be defined. Appendix A brings together these different elements and presents the comprehensive basis for these curves. These elements include the laboratory data used by GENE in disposition efforts, data used to discuss the SCC behavior of Ni-base alloys with the NRC, field cracking data, crack growth data from other laboratories and the fundamental PLEDGE model based on stress corrosion principles. This chapter presents the key information from Appendix A and presents the Disposition Curves to be used in the analysis of crack deepening.

5.1 Review of Alloy 182 Disposition Efforts

In response to the cracking in the nozzle-to-safe-end locations and the access hole covers, several utilities required disposition actions to evaluate the consequences of crack growth on the structural margin of the component [16-18]. These analyses were plant specific and directed at the particular cracking conditions found in the components. In some cases, a generic methodology was also invoked. These included a generic report that was prepared for the BWR Owner's Group for Access Hole Covers as well as several specific analyses of nozzle-to safe-end cracking [19-20 . In each analysis the basis for the crack growth rates was presented. Specific discussions of crack growth rates for Alloy 182 and Alloy 600 wrought materials were given. Analyses based on crack growth rates at or below 5×10^{-5} in/hr were used to support operation for additional fuel cycles. These evaluations are useful not only because of the field experience

documentation, but also because of the precedent of NRC acceptance of the crack growth rate basis.

5.2 Rates Determined From Field Cracking Events

As stated, cracking has been detected in several different plants in BWR piping components constructed with Alloy 182. Many of the safe ends were overlayed or repaired immediately. Appendix A gives the UT determined crack depth data for many of the crack indications in the different nozzle-to-safe-end welds. Data is also presented for the limited number of re-inspections. The total data base is quite large and can be used to estimate average crack growth rates.

Using the nozzle-to-safe-end cracking incidents, crack growth rates can be estimated by making assumptions on crack initiation time or using reinspection data. Since many of the Alloy 182 cracks are associated with weld defects or weld repairs, the crack initiation time is negligible and field data on crack depths can be used to estimate crack growth over the actual hot operating time. The rate calculations include the initial inspection data as well as the data from the nozzles that were re-inspected. The UT estimated depths and crack growth rates are given in Appendix A. These results provide actual estimates of average crack growth rates under actual plant operating environments. Since many of the cracks were found in plants that had poor conductivity in the first five operating cycles the assumption of very early initiation is reasonable.

Content Deleted - EPRI Proprietary Information

5.3 Review Of Recent Data

As a significant part of crack growth assessment efforts, GENE made use of CAVS data to support specific disposition efforts as well as to continually benchmark/validate the conservative nature of its proposed crack growth rates for Alloy 182 and Alloy 600. There have also been continuing efforts to compile laboratory crack growth rate data that have been measured throughout the industry. This compilation now includes data from ABB, Studsvik, VTT, Toshiba and GE CR&D which complements the other existing GENE data. These data are compared with the previous GENE efforts in the second section. The CAVS data has continued

to be useful in benchmarking the behavior of Alloy 182 under plant water chemistry conditions. The conductivity level, the specific anionic species and the types of oxidizing species which are present in the in-reactor environment tests have been difficult to reproduce in most laboratory settings.

The EPRI/BWRVIP has recently spent significant effort collecting and reviewing much of the Alloy 182 data from the different testing laboratories to better assess the rates of crack growth. The data covers a large range of conductivity, corrosion potential, cyclic loading conditions and applied K level. It is appropriate that this data also be reviewed for consistency with any proposed disposition curve. Applying the appropriate screens (to exclude data for conditions that are outside the range expected in plant operation) which included conductivity level, constant load conditions, limitation on applied K and limitations on data with large post-test corrections, the data set is consistent with the GENE laboratory and CAVS data.

Content Deleted –
EPRI Proprietary Information

5.4   Modeling Assessments

The working hypothesis for the crack propagation process for IGSCC of Ni-base alloys is widely acknowledged to be similar to that for type 304/316 austenitic stainless steel in high temperature water. For Alloy 182 weldments, the weld residual stress, the Alloy 182 material susceptibility, and the oxygenated water environment are factors that lead to IGSCC cracking. The GE PLEDGE model makes use of these fundamental inputs and has been used to evaluate crack growth and factors of improvement based on environmental parameters.

5.5   Disposition Crack Growth Rate Approach

Using all of this background understanding, the disposition curves incorporate two additional considerations. First there is a clear recognition that the coolant environment, particularly its corrosion potential and conductivity directly influence crack growth rates. Therefore, curves are developed for three different environments: (1) Normal Water Chemistry at or below EPRI Action Level 1 conditions, (2) high purity Normal Water Chemistry with conductivity restricted

to 0.15 S/cm or better and sulfate and chloride levels below 5 ppb consistent with EPRI Action Level 1 and (3) Hydrogen Water Chemistry that meets EPRI guidelines. The second key element in the methodology for these proposed disposition curves is an approach similar to that proposed in BWRVIP-14 for dispositioning stainless steel.

Content Deleted -
EPRI Proprietary Information

5.6   Specific Curves

Based on all of the past and current information, Disposition Crack Growth Rate Curves are proposed for the evaluation Alloy 182 crack growth for each of three different environments: (1) normal water chemistry (NWC) that meets the EPRI Water Chemistry Guidelines, (2) a more restrictive NWC with conductivity at or better than 0.1 S/cm and (3) hydrogen water chemistry (HWC) that meets EPRI guidelines. These curves are to be used for through thickness growth.

5.6.1   Normal Water Chemistry Below EPRI Guidelines Action Level 1

Figure 5-1 displays the proposed curve for use under these NWC conditions.

Content Deleted -
EPRI Proprietary Information

**Content Deleted -
EPRI Proprietary Information**

5.6.2 Normal Water Chemistry with Conductivity At or Below 0.15 S/cm

The second Disposition Crack Growth Rate Curve is to be used for high purity NWC environments where the average cycle conductivity is 0.15 S/cm or better and the sulfate and chloride levels do not exceed 5 ppb during the assessment period.

**Content Deleted -
EPRI Proprietary Information**

5.6.3 Hydrogen Water Chemistry within EPRI Guidelines

The benefits of HWC have been repeatedly shown as discussed in this report and other references. For the time on HWC, lower crack growth rates can be used.

**Content Deleted -
EPRI Proprietary Information**

5.6.4   Crack Growth Rates for Assessing Crack Lengthening

**Content Deleted -
EPRI Proprietary Information**

**Content Deleted -
EPRI Proprietary Information**

Figure 5-1. Proposed Disposition Curve for NWC at or Below Action Level 1

**Content Deleted -
EPRI Proprietary Information**

Figure 5-2. Proposed NWC Disposition Curve CAVS Data and Old GENE Lab Data

Content Deleted -
EPRI Proprietary Information

Figure 5-3. NWC Disposition Curve vs. Screened BWRVIP Alloy 182 Data

**Content Deleted -
EPRI Proprietary Information**

Figure 5-4. Comparison of NWC Curve with Field Inspection Field Data

**Content Deleted -
EPRI Proprietary Information**

Figure 5-5. Proposed High Purity NWC Disposition Curve

**Content Deleted -
EPRI Proprietary Information**

Figure 5-6. Comparison of High Purity NWC Disposition Curve with Screened Lab and CAV Data

**Content Deleted -
EPRI Proprietary Information**

Figure 5-7. HWC Disposition Curve Compared with CAVS and Lab Data Under HWC Conditions

6.0 CRACK GROWTH EVALUATION

In this section, crack growth evaluation is performed for all the various welds of the core shroud support structure of a BWR-6 using the crack growth disposition curves provided in Section 5 and the K distribution for the individual welds determined in Section 4. The basic formulation of the crack growth disposition curve for any of the water chemistry conditions provided in Section 5 is given by

**Content Deleted -
EPRI Proprietary Information**

The results of the evaluation are presented in Tables 6-2 through 6-6. The following provides a summary of the observations on the evaluation results.

**Content Deleted -
EPRI Proprietary Information**

**Content Deleted -
EPRI Proprietary Information**

Table 6-1

Crack Growth Evaluation Input

Weld	Thickness (in)	K Distribution	Crack Growth Disposition Curve	Initial Flaw Size (in)
H-8 (Top-to-Bottom)	2.5	Figure 4-1	NWC (Fig. 5-2) High Purity NWC (Fig. 5-5) HWC (Fig. 5-7)	0.25
H8 (Bottom-to-Top)	2.5	Figure 4-2	NWC (Fig. 5-2) High Purity NWC (Fig. 5-5) HWC (Fig. 5-7)	0.25
H9 (Top-to-Bottom)	2.5	Figure 4-3	NWC (Fig. 5-2) High Purity NWC (Fig. 5-5) HWC (Fig. 5-7)	0.25
H9 (Bottom-to-Top)	2.5	Figure 4-4	NWC (Fig. 5-2) High Purity NWC (Fig. 5-5) HWC (Fig. 5-7)	0.25
H10	3.0	Figure 4-9	NWC (Fig. 5-2) High Purity NWC (Fig. 5-5) HWC (Fig. 5-7)	0.30
H11	5.0	Figure 4-11	NWC (Fig. 5-2) High Purity NWC (Fig. 5-5) HWC (Fig. 5-7)	0.50
H12	5.0	Figure 4-13	NWC (Fig. 5-2) High Purity NWC (Fig. 5-5) HWC (Fig. 5-7)	0.50

Table 6-2

Crack Growth Evaluation Results for Weld H8

**Content Deleted -
EPRI Proprietary Information**

Table 6-3

Crack Growth Evaluation Results for Weld H9

**Content Deleted -
EPRI Proprietary Information**

Table 6-4

Crack Growth Evaluation Results for Weld H10

**Content Deleted -
EPRI Proprietary Information**

Table 6-5

Crack Growth Evaluation Results for Weld H11

**Content Deleted -
EPRI Proprietary Information**

Table 6-6

Crack Growth Evaluation Results for Weld H12

**Content Deleted -
EPRI Proprietary Information**

7.0   SUMMARY AND CONCLUSION

The following provides a summary and conclusions of the work performed in this report to support crack growth evaluation of the nickel base austenitic alloy core shroud support welds H8, H9, H10, H11 and H12.

Empirical through-wall crack growth disposition curves have been proposed for various water chemistry conditions for use in the evaluation of BWR nickel base austenitic alloys in RPV internals. The disposition curves are of the form:

**Content Deleted -
EPRI Proprietary Information**

A comprehensive study was performed to determine the through-wall residual stress distributions for the various welds of the shroud support structure. These included welds H8, H9, H10, H11 and H12 of a BWR-5, 6 design. Both experimental and analytical techniques were used to determine the residual stress distributions. When the analytical results were adjusted to account for the parting out stresses, there was good agreement between the analytical and the experimental results.

The through-wall weld residual stresses were used in a fracture mechanics analysis to determine the weld specific through-wall stress intensity factor distributions for welds H8, H9, H10, H11 and H12.

**Content Deleted -
EPRI Proprietary Information**

The crack growth disposition curves and the stress intensity factor distributions were used to perform crack growth evaluations for the individual welds.

**Content Deleted -
EPRI Proprietary Information**

The evaluation results presented in this report are conservative in that they did not take into consideration the long initiation time to cracking exhibited by these nickel base austenitic alloys under non-creviced conditions. To date, only one incidence of minor cracking has been observed in a core shroud support structure weld.

Even though the residual stresses were determined for a BWR-6 design, it is believed that the results of this report and a companion report for the reactor pressure vessel currently under preparation can be used to address the support structure welds of other BWR designs.

8.0 REFERENCES

1. EPRI Report No. TR-105707, BWR Vessel and Internals Project, "Safety Assessment of BWR Reactor Internals (BWRVIP-06)," EPRI PROPRIETARY, October 1995.

2. EPRI Report No. TR-105873, BWR Vessel and Internals Project, "Evaluation of Crack Growth in BWR Stainless Steel RPV Internals (BWRVIP-14)," EPRI PROPRIETARY, March 1996.

3. EPRI Report No. TR-104972, "Stress Corrosion Cracking of Alloys 600 and 182 in BWRs," September 1994.

4. EPRI Report No. NP-2617, "Stress Corrosion Cracking in Alloy 600 and 690 and Weld Metals No. 82 and 182 in High-Temperature Water," September 1982.

5. EPRI Report no. NP-5882M, "Stress Corrosion Cracking Resistance of Alloys 600 and 690 and Compatible Weld Metals in BWRs," July 1988.

6. NUREG-0313, Revision 2, "Technical Report on Material Selection and Processing Guidelines for BWR Coolant Pressure Boundary Piping," U. S. Nuclear Regulatory Commission, January 1988.

7. Hettiarachchi, S. et.al., "The Concept of Noble Metal Chemical Addition Technology for IGSCC Mitigation of Structural Materials," NACE International, Seventh International Symposium on Environmental Degradation of Materials in Nuclear Power Systems - Water Reactors, August 7-10, 1995, Breckenridge, CO.

8. BWRVIP Document, "Vessel Internals Inspection Summaries," EPRI PROPRIETARY, April 1997.

9. EPRI Report No. TR-108823, BWR Vessel and Internals Project, "BWR Shroud Support Inspection and Flaw Evaluation Guidelines (BWRVIP-38)," EPRI PROPRIETARY, September 1997.

10. EPRI Report No. TR-108709, BWR Vessels and Internals Project, " Evaluation of Stress Corrosion Crack Growth in Low Alloy Steel Vessel Materials in the BWR Environment" (BWRVIP-60)," EPRI PROPRIETARY, March 1999.

11. EPRI Repair and Replacement Application Center, "Stress Analysis of River Bend Unit 2 Reactor Pressure Vessel and Alloy 600 Weld Components".

12. ANSY Finite Element Program, Revision 5.3, Swanson Analysis Systems, Inc.

13.	ASME Boiler and Pressure Vessel Code, Section XI, 1995 Edition

14.	Cipolla, R. C., "Technical Basis for the Revised Stress Intensity Factor Equation for Surface Flaws in ASME Section XI Appendix A," Proceedings of ASME Pressure Vessels and Piping Conference, PVP-Vol. 313-1, July 1995.

15.	Cheng, W., "Determination of the Stress Intensity Factor for an Edge-Cracked Beam with Fixed Ends" to be submitted to *Engineering Fracture Mechanics*.

16.	General Electric Nuclear Energy report SASR 89-18, "Brunswick Nozzle Cracking," February 1989.

17.	General Electric Nuclear Energy report SASR 89-22: " Evaluation of the Indication in the Limerick Unit 1 H2H Safe End to Nozzle Weld," August 1989.

18.	General Electric Nuclear Energy report SASR-89-37: " Evaluation of the Indication in the River Bend Feedwater Nozzle to Safe End Weld," May 1989.

19.	General Electric Nuclear Energy report PMWG-G-537, "Update of Nozzle/Alloy 182 Butter Cracking," 1989.

20.	General Electric Nuclear Energy report 523-107-0892: "BWR Access Hole Cover Radial Cracking Evaluation," October 1992.

APPENDIX A

NICKEL BASE CRACK GROWTH DISPOSITION CURVES

Nickel Base Crack Growth Disposition Curves

Prepared for

Electric Power Research Institute

Prepared by:

RM Horn

GE Nuclear Energy
175 Curtner Avenue
San Jose, CA 95125

PROPRIETARY INFORMATION NOTICE

This document contains proprietary information of the General Electric Company (GE) and is furnished to the Electric Power Research Institute (EPRI) in confidence solely for the purpose or purposes stated in the transmittal letter. No other use, direct or indirect, of the document or the information it contains is authorized. EPRI shall not publish or otherwise disclose it or the information to others without written consent of GE.

IMPORTANT NOTICE REGARDING

CONTENTS OF THIS REPORT

Please read carefully

The only undertakings of the General Electric Company (GE) respecting information in this document are contained in the contract between EPRI and GE, and nothing contained in this document shall be construed as changing the contract. The use of this information by anyone other than EPRI with respect to any unauthorized use, GE makes no representation or warranty, express or implied, and assumes no liability as to the completeness, accuracy, or usefulness of the information contained in this document, or that its use may not infringe upon privately owned rights.

EXECUTIVE SUMMARY

The ability to predict the crack depth changes of an existing crack indication requires the use of a crack growth rate curve. The purpose of this report is to present the basis for intergranular stress corrosion crack (IGSCC) growth rate disposition curves that can be used with Nickel based structural alloys, Alloy 182 weld metal and Alloy 600 wrought material.

Beginning in the 1970s and continuing to the present, General Electric Nuclear Energy (GENE) has performed studies of the behavior of these Nickel based structural materials that are used throughout BWRs. These studies have included laboratory stress corrosion tests including initiation and crack growth tests, and in reactor site tests and failure analyses investigations GENE has also continued to accumulate data bases on field behavior of these materials from in-service inspections, and has continually been involved with evaluating plant cracking. These efforts have included dispositioning indications for specific utilities in the limited cases where cracking has been detected. GE has also discussed the IGSCC susceptibility of these alloys with the NRC on a regular basis to aid in the dissemination of data and understanding IGSCC prediction.

Using this foundation, this report has been prepared to define interim disposition crack growth rate curves for use with Alloy 182 components. The report brings together these different elements that when taken together provide a solid basis for these curves. These elements include the laboratory data used by GENE in disposition efforts, IGSCC data on the behavior of Ni-base alloys discussed with the NRC, field cracking data, crack growth data from other laboratories and the fundamental PLEDGE model based on stress corrosion principles.

The methodology has two important elements to it. First there is a clear recognition that the coolant environment, particularly its corrosion potential and conductivity directly influence crack growth rates. Therefore, curves are developed for three different environments: (1) Normal Water Chemistry at or below EPRI Action Level 1 conditions, (2) Normal Water Chemistry with high purity set by restricting conductivity to 0.15 S/cm or better and sulfate and chloride levels to 5 ppb or less, and (3) Hydrogen Water Chemistry that meets EPRI guidelines. The second key element in the methodology for these interim disposition curves is an approach similar to that proposed in BWRVIP-14 for dispositioning stainless steel.

A-4

**Content Deleted -
EPRI Proprietary Information**

As stated, this report presents the technical basis for the methodology and the environmentally based rates. It discusses both old and new laboratory data, field experience and previous interactions with the NRC and on PLEDGE model relationships.

**Content Deleted -
EPRI Proprietary Information**

Clearly, there is a continuing need to generate additional laboratory data to resolve the uncertainties in current information resulting from the variability in the techniques used to perform earlier crack growth studies. These future data will aid in refining the interim approaches and can be used in developing long term predictive capabilities for accurate plant specific evaluations.

TABLE OF CONTENTS

BACKGROUND

Alloy 182 is known to be susceptible to stress corrosion cracking (SCC) in high temperature oxygenated water environment (Reference 1). Alloy 182 cracking was first discovered in a US BWR/3 plant at the recirculation nozzle safe end weld during safe end replacement. Since then, there have been several instances of cracking at nozzle-to-safe-end welds (Reference 2). More recently, cracking was found in Alloy 182 attachment welds related to reactor internals. Because of the extensive use of Alloy 182 in BWR internals and the difficulty of repair or replacement, Alloy 182 cracking is a significant issue that requires a well defined methodology to allow evaluation of crack indications.

The best accepted working hypothesis for the crack propagation process for IGSCC of Ni-base alloys follows that for type 304/316 austenitic stainless steel in high temperature water.

Content Deleted - EPRI Proprietary Information

There have been many evaluations within GE Nuclear Energy (GENE) of Ni-base Alloys, particularly Alloy 182. These have included assessment of field cracking, laboratory crack initiation and crack growth tests, component tests and in-reactor crack growth tests. The objective of the work has been directed at assessing the susceptibility to IGSCC as a function of material condition, composition and water chemistry parameters. Crack growth tests have been performed to evaluate the effects of normal water chemistry as well as hydrogen water chemistry.

With the recent efforts in developing Noble Metal Technology with special emphasis on Noble Metal Chemical Addition (NobleChem), there have also been significant levels of testing to demonstrate IGSCC mitigation in Alloy 182 under NMCA/HWC (Reference 6). GE has also maintained a continuing awareness of other efforts to assess crack growth behavior in these susceptible materials.

The purpose of this report is to summarize all of the relevant GE Nuclear Energy information to support crack growth rate curves that could be used to assess crack growth in Alloy 182 material used in the BWR reactor internals components. This report will draw on historical information, field experience and the current understanding of crack growth test data to develop these proposed disposition curves. This proprietary GE report will serve as the technical basis for GE's proposed crack growth rates, which will be used in the EPRI/BWRVIP report on Alloy 182. The EPRI/BWRVIP report will describe a generic methodology to disposition crack indications that might be detected in the Alloy 182 regions of reactor internal components. The purpose of this approach is to propose these conservative disposition curves with the understanding that the critical aspects of crack growth behavior of Alloy 182 will be better clarified and quantified using modern techniques in future efforts.

REPORT OUTLINE

The report will include the following sections. First there will be a review of previous plant specific evaluation of crack indications in components constructed using Alloy 182. These evaluations were concentrated in the late 1980s when cracking was detected in Alloy 182 nozzle-to-safe-end weld butters. Second, GENE had continuing dialogue on the susceptibility and crack

growth rates in Alloy 182. The next section will summarize these meetings between GENE and the NRC.

The third section will review field cracking in Alloy 182 and will document the understanding of crack growth as determined by destructive evaluation as well as ultrasonic inspection. The fourth section will present the crack growth data base that was developed by GE. This data will cover laboratory data as well as data that was measured in the GE CAV systems. This material will provide a understanding of the efforts used as a basis for short term disposition of Alloy 182 cracking in operating plants. The final section will review the current, more comprehensive crack growth data base that has been assembled by EPRI and which includes data from a variety of testing laboratories throughout the world.

Based on all of this information, the report will develop three crack growth rate curves that can be used in assessments of crack growth in reactor internals. This section will describe the constraints that need to be applied while using these growth rate curves. These special considerations include the type of stresses that drive SCC and the time period for the application of the rates. The proposed interim crack growth rate curves consider different plant operating environments, particularly normal water chemistry (NWC) and hydrogen water chemistry (HWC). They will be inputs to the BWRVIP report on Alloy 182 weld metal and will therefore undergo utility and EPRI review.

REVIEW OF PREVIOUS EFFORTS TO EVALUATE ALLOY 182 CRACKING IN OPERATING BWRS

**Content Deleted -
EPRI Proprietary Information**

**Content Deleted -
EPRI Proprietary Information**

Review of Alloy 182 Disposition Efforts

**Content Deleted -
EPRI Proprietary Information**

**Content Deleted -
EPRI Proprietary Information**

Historical Disposition Crack Growth Discussion

Limerick 1: First Disposition Effort: 1989

**Content Deleted -
EPRI Proprietary Information**

Hatch Access Hole Cover Disposition

**Content Deleted -
EPRI Proprietary Information**

**Content Deleted -
EPRI Proprietary Information**

Limerick 1: Follow-up Disposition Effort: 1990

**Content Deleted -
EPRI Proprietary Information**

**Content Deleted -
EPRI Proprietary Information**

DISCUSSIONS WITH THE US NRC ON ALLOY 182 CRACK GROWTH RATES

**Content Deleted -
EPRI Proprietary Information**

IGSCC Technology Update Meeting for NRC: June 9, 1987

**Content Deleted -
EPRI Proprietary Information**

**Content Deleted -
EPRI Proprietary Information**

RATES DETERMINED FROM FIELD CRACKING EVENTS

As stated in Section 3 and listed in Table A-2, cracking has been detected in several different plants in BWR piping components constructed with Alloy 182. Many of the safe ends were overlayed or repaired immediately. Table A-5 gives the UT determined crack depth data for many of the crack indications in the different nozzle-to-safe-end welds. Table A-6 gives data from the limited number of re-inspections. The total data base is quite large.

The information on cracking in BWR core internal structures is very limited, due in large part to the small number and the extent of inspections that have occurred to date. Many of the utilities have performed selective inspections as a part of local lower plenum inspections or in conjunction with shroud repairs.

**Content Deleted -
EPRI Proprietary Information**

**Content Deleted -
EPRI Proprietary Information**

REVIEW OF RECENT DATA

As a significant part of crack growth assessment efforts, GENE made use of CAV data to support specific disposition efforts as well as to continually benchmark/validate the conservative nature of its proposed crack growth rates for Alloy 182 and Alloy 600. Some of these data are listed in the earlier sections. However, GE has continued to compile data from the different plants to be used in this way. These data are reviewed in the next section.

There have also been continuing efforts to compile laboratory crack growth rate data that have been measured throughout the industry. This compilation now includes data from ABB, Studsvik, VTT, Toshiba and GE CR&D which complements the other existing GENE data. These data are compared with the previous GENE efforts in the second section.

Recent CAV Data

**Content Deleted -
EPRI Proprietary Information**

Content Deleted -
EPRI Proprietary Information

Recent Crack Growth Rate Data

Content Deleted -
EPRI Proprietary Information

Recent GENE Crack Growth Rates Efforts

Content Deleted -
EPRI Proprietary Information

**Content Deleted -
EPRI Proprietary Information**

MODELING ASSESSMENTS

**Content Deleted -
EPRI Proprietary Information**

Content Deleted -
EPRI Proprietary Information

PROPOSED INTERIM DISPOSITION CURVES

Review of Basis for Approach

The purpose of this report is to establish the basis for proposed disposition curves for Alloy 182 weld metal. These curves are primarily for crack growth prediction in the radial or through thickness direction, not for crack lengthening. By presenting a historical perspective of previous

disposition efforts, previous GENE/NRC discussions on the behavior of these susceptible materials as well as the field determined crack growth behavior, these interim curves will build on the current understanding. The report also reviews all of the available crack growth rate data. This includes the early GENE data, old and updated CAV data, compilation all of the laboratory data and the results of recent laboratory tests performed by GE CR&D and GENE. The final element is information from modeling efforts that build on peer reviewed fundamental approaches to calculating crack growth rates for ductile austenitic materials which are susceptible to SCC.

When put together, this information provides a comprehensive basis for dispositioning reactor internal components where cracking might occur in Alloy 182 weld material and might continue to grow into Ni-base materials. However, it is also important to add limitations on the broad applicability of these disposition curves.

**Content Deleted -
EPRI Proprietary Information**

Specific Curves

Curves are proposed for the evaluation Alloy 182 crack growth for each of the three different environments. These environments include (1) normal water chemistry (NWC) that meets the EPRI Water Chemistry Guidelines, (2) a more restrictive NWC with conductivity at or better than 0.15 S/cm and sulfate and chloride levels less than 5 ppb and (3) operation with fully effective HWC. The proposed curves will be discussed and presented separately for each operational environment.

Normal Water Chemistry Below EPRI Guidelines Action Level 1

**Content Deleted -
EPRI Proprietary Information**

Normal Water Chemistry with Conductivity Below 0.15 S/cm

**Content Deleted -
EPRI Proprietary Information**

Hydrogen Water Chemistry within EPRI Guidelines

**Content Deleted -
EPRI Proprietary Information**

Comparison with PLEDGE and the SKI Disposition Curves

It is useful to compare the three disposition curves with the GE PLEDGE model predictions. All three curves are plotted along with the comparable PLEDGE calculations in Figure A-30.

**Content Deleted -
EPRI Proprietary Information**

Applicability to Alloy 600

**Content Deleted -
EPRI Proprietary Information**

CONCLUSIONS AND RECOMMENDATIONS

Based on the study of SCC crack growth rates in Nickel Base Alloy 182 weld metal and Alloy 600 wrought material presented in this report, the following conclusions can be made.

**Content Deleted -
EPRI Proprietary Information**

Content Deleted -
EPRI Proprietary Information

REFERENCES

1.   A Page: "Stress Corrosion Cracking of Alloys 600 and 690 and Weld Metals No. 82 and 182 in High Temperature Water," EPRI NP-2617, September 1982.

2.   "Pilgrim Nuclear Power Station Recirculation Nozzle Repair Program and Hydrogen Water Chemistry Materials Qualification," GENE NEDC-30730-P, September 1984.

3.   FP Ford and PL Andresen: Development and Use of a Predictive Model of Crack Propagation in 304/316L, A533B and Inconel600/182 Alloys in 288oC Water, "Proc. 3rd Int. Conf. On Environmental Degradation of Materials in Nuclear Power Plants - Water Reactors, Traverse City, August 1987, NACE, Houston.

4.   PL Andresen: Observation and Prediction of the Effects of Water Chemistry and Mechanics on Environmentally Assisted Cracking of Inconel 182 Weld Metal and 600,", Corrosion 44, 6, 1988, p.376.

5.   EL Hall and CL Briant: "The Microstructural Response of Mill Annealed and Solution Annealed Inconel 600 to Heat Treatment," Met Trans. A, vol. 16A, p1225, 1985.

6.   S. Hettiarachchi, G. P. Wozadlo, P. L. Andresen, T. P. Diaz, and R. L. Cowan, The Concept of Noble Metal Chemical Addition Technology for IGSCC Mitigation of Structural Materials, Proc. 7th int. Conf. on Environmental Degradation of Materials in Nuclear Power Systems- Water Reactors, National Association of Corrosion Engineers, 1995.

7.   GENE Service Information Letter 455: "Recommendation For Additional In-service Inspection Of Alloy 182 Nozzle Welds," S455r1, GE Nuclear Energy - San Jose, California; February 22, 1988.

8.   Brunswick Nozzle Cracking: GENE SASR 89-18, dated February 1989.

9.   GENE PMWG-G-537: Update of Nozzle/Alloy 182 Butter Cracking, 1989.

10. GENE 523-107-0892: "BWR Access Hole Cover Radial Cracking Evaluation," October 1992.

11. GENE SASR 89-22: " Evaluation of the Indication in the Limerick Unit 1 H2H Safe End to Nozzle Weld," August 1989.

12. GENE SASR-89-37: " Evaluation of the Indication in the River Bend Feedwater Nozzle to Safe End Weld," May 1989.

13. GENE 523-113-0892: "Hatch Access Hole Cover Assessment," August 1992.

14. GENE SASR 90-95: "Summary Report of the Evaluation of the Recirculation Nozzle to Safe End Weld Indication and Proposed Disposition to Permit Unit 1 Cycle 4 Operation," December 1990.

15. CW Jewett: GENE NEDE-31618P, October 1988.

16. MM Bensch: GENE PMT Transmittal 83-509-015, February 1983.

17. RM Horn: GENE PMWG-G353, January 1984.

18. DA Hale, CW Jewett and CS O'Toole: GENE NEDE-31110, November 1985.

19. Peach Bottom Unit 2 GENE Interim CAV Reports: September 1986 - January 1987.

20. Brunswick Unit 2 GENE Interim CAV Reports: October 1988-June 1989.

21. Duane Arnold Energy Center GENE Interim CAV Reports: September 1987-September 1992.

22. FitzPatrick GENE Interim CAV Reports: January 1988-March 1990.

23. Hatch Unit 1 GENE Interim CAV Reports: 1990-1991.

24. Brunswick Unit 1 GENE Interim CAV Reports: January-May 1990.

25. Limerick Unit 1 GENE Interim CAV Reports: 1989-1991.

26. Nuclenor GENE Interim CAV Reports: September 1989.

27. Pilgrim GENE Interim CAV Reports: March-June 1990.

28. LG Ljungberg: "Stress Corrosion Cracking of Alloys 600 and 182 in BWRs," EPRI/SKI Research Project 2293-1, Interim Reports: 1991-1994.

29. PL Andresen: GENE PMWG G-566, March 1990.

30. Private communication: PL Andresen.

31. "Evaluation of Crack Growth in BWR Stainless Steel RPV Internals (BWRVIP-14)," EPRI TR-105873, March 1996.

32. K. Gott: "Using Materials Research Results in New Regulations - The Swedish Approach," Proc. 7rd Int. Conf. On Environmental Degradation of Materials in Nuclear Power Plants - Water Reactors, Breckenridge, Colorado, August 1995, NACE, Houston.

**Content Deleted -
EPRI Proprietary Information**

Table A-1: Pilgrim Nozzle Cracking Data

**Content Deleted -
EPRI Proprietary Information**

Table A-2: Lists of Plants with Nozzle/Safe End Cracking

**Content Deleted -
EPRI Proprietary Information**

Table A-3: Summary of Access Hole Cover Cracking in US Plants

**Content Deleted -
EPRI Proprietary Information**

Table A-4: GENE Efforts in Evaluating and Dispositioning Cracking in

Alloy 182 Welds

**Content Deleted -
EPRI Proprietary Information**

Figure A-1: Alloy 182 Crack Growth Rate Dependency (References 15-18)

Content Deleted -
EPRI Proprietary Information

Figure A-2: Alloy 182 Crack Growth Rate Dependency with Conductivity

**Content Deleted -
EPRI Proprietary Information**

Figure A-3: Crack Growth Rates for Alloy 182 (<0.5 µS/cm) (References 19-28)

**Content Deleted -
EPRI Proprietary Information**

Figure A-4: SCC Crack Growth Rates for Alloy 182 (<0.5µS/cm and >0.5µS/cm: ref.19-26)

**Content Deleted -
EPRI Proprietary Information**

**Figure A-5: SCC Crack Growth Rates for Nickel Base Alloys as a Function of
Conductivity (Reference 29)**

A-36

**Content Deleted -
EPRI Proprietary Information**

Figure A-6: SCC Crack Growth Rates for Alloy 600

**Content Deleted -
EPRI Proprietary Information**

Figure A-7: CAVS Alloy 182 Data: Limerick 1

Content Deleted -
EPRI Proprietary Information

Figure A-8: CAVS Data From Various Plants (References 19-25).

**Content Deleted -
EPRI Proprietary Information**

Figure A-9: Comparison of the Predicted and Observed Rates vs. Stress Intensity for
Data on Alloy 182 (References 19-25)

Content Deleted -
EPRI Proprietary Information

Table A-5: Field Cracking Data for Nozzle-to-Safe End Alloy 182: Initial Inspection

**Content Deleted -
EPRI Proprietary Information**

Table A-6a: Field Cracking Data for Nozzle-to-Safe End Alloy 182 after re-inspection

**Content Deleted -
EPRI Proprietary Information**

Table A-6b: Field Cracking Data for Nozzle-to-Safe End Alloy 182 after second re-inspection

**Content Deleted -
EPRI Proprietary Information**

**Figure A-10: Field Inspection Crack Growth Rate Data
(as a function of time when inspection was performed)**

**Content Deleted -
EPRI Proprietary Information**

Figure A-11: Inspection Field Data: Axial and Circumferential Nozzle Cracking

**Content Deleted -
EPRI Proprietary Information**

Figure A-12: GENE lab and CAV data vs. K level

**Content Deleted -
EPRI Proprietary Information**

Figure A-13: CAVS Data along with GENE Disposition Band

**Content Deleted -
EPRI Proprietary Information**

Figure A-14: Alloy 600 CAVS Data (all ECP conditions)

**Content Deleted -
EPRI Proprietary Information**

Figure A-15: Full BWRVIP Alloy 182 Data Base

**Content Deleted -
EPRI Proprietary Information**

Figure A-16: BWRVIP Alloy 182 Data Screened by GE

**Content Deleted -
EPRI Proprietary Information**

Figure A-17: CAVS Data under HWC Conditions

**Content Deleted -
EPRI Proprietary Information**

Figure A-18: Alloy 600 CAVS Data (ECP < -230mV,she)

**Content Deleted -
EPRI Proprietary Information**

Figure A-19: Crack Growth Rates for Alloy 182 Compared with PLEDGE
Predictions

**Content Deleted -
EPRI Proprietary Information**

Figure A-20: PLEDGE Calculations vs. Proposed NWC Disposition Curve

Content Deleted -
EPRI Proprietary Information

Figure A-21: Proposed Disposition Curve for NWC at or below Action Level 1

A-53

**Content Deleted -
EPRI Proprietary Information**

Figure A-22: Proposed NWC Disposition Curve vs. GENE CAV and lab data

**Content Deleted -
EPRI Proprietary Information**

Figure A-23: NWC Disposition Curve vs. Screened BWRVIP Alloy 182 Data

**Content Deleted -
EPRI Proprietary Information**

Figure A-24: Comparison of NWC Curve with Field Inspection Field Data

A-56

**Content Deleted -
EPRI Proprietary Information**

Figure A-25: Proposed High Purity NWC Disposition Curve

**Content Deleted -
EPRI Proprietary Information**

Figure A-26: Proposed NWC Disposition Curves with CAVS Data and old GENE Curves

A-58

**Content Deleted -
EPRI Proprietary Information**

Figure A-27: Comparison of High Purity NWC Disposition Curve with screened lab and CAV
data

**Content Deleted -
EPRI Proprietary Information**

Figure A-28: Proposed HWC Disposition Curve

A-60

**Content Deleted -
EPRI Proprietary Information**

**Figure A-29: HWC Disposition Curve Compared with CAVS and Lab Data under HWC
Conditions**

**Content Deleted -
EPRI Proprietary Information**

Figure A-30: PLEDGE Calculations vs. Proposed Curves

**Content Deleted -
EPRI Proprietary Information**

Figure A-31: Proposed Disposition Curves vs. SKI Curves

APPENDIX B

THROUGH-THICKNESS RESIDUAL STRESS MEASUREMENT AT

RIVER BEND NUCLEAR STATION

Prepared by:

W. Cheng

University of California, Berkeley

(Currently with Berkeley Engineering and Research)

Measurements of Residual Stresses in BWR Core Shroud Support Welds

Research Project B301-11

Final Report, December 1997

Prepared by

Weili Cheng
Iain Finnie
University of California, Berkeley
Berkeley, CA 94720

Table of Contents

List of Tables

ii

List of Figures

1.0 INTRODUCTION

The presence of residual stresses due to welding has been found to have a significant influence on the intergranular stress corrosion cracking (IGSCC) BWR vessel internals. The objective of the project is to use the crack compliance method to obtain the residual stresses in the BWR core shroud support welds H8, H10 and H9, and H12. A brief overview of the theoretical background and experimental procedures of the method is given in this section. The results of measurement for different welds will then be presented.

1.1 Theoretical Background

The crack compliance method is based on linear superposition for the linear elastic deformation which occurs when a thin cut of progressively increasing depth is introduced into a body with residual stresses. That is, the deformation due to releasing residual stresses, as shown in Fig. 1, is the same as that produced by applying the same stress with opposite sign to the faces of the cut.

The unknown residual stress distribution released by cutting is first represented by a series

$$\sigma(x) = \sum_{i=0}^{n} A_i P_i(x) \tag{1}$$

in which A_i is the amplitude factor to be determined for the ith term of a prescribed polynomial series $P_i(x)$. When the change of strain ε is measured for a given depth of cut a, as shown in Fig. 2, the relation between the stress released and the strain measured may be expressed as

$$\varepsilon(a) = \sum_{i=0}^{n} A_i C_i(a) \tag{2}$$

where $C_i(a)$, referred to as the crack compliance function, is the strain produced by the surface traction $P_i(x)$ for a depth of cut a. When a number $m > n-1$ of strain measurements are made, a least squares fit can be used to minimize the mean error involved in the measurement and estimation. This procedure leads to a set of $n-1$ linearly independent equations, from which the unknown A_i can be solved.

For through-thickness measurement the cut can be approximated by a crack and the crack compliance functions are obtained for an edge-cracked body subjected to an arbitrary surface traction

on the crack faces [1]. To ensure zero resultant force and moment over the thickness, the residual stress distribution is usually approximated by Legendre polynomials of orders larger than one. For a body of a complicated geometry, the finite element method can be used to carry out the required computations.

1.2 Experimental Procedures

Strain gages are first installed on specimens at locations optimal for measurement of residual normal stresses. Electrical discharge wire machining (EDWM) is then used to introduce a thin cut of increasing depth as shown in Fig 2. The test is carried out in a temperature-controlled environment. For through-thickness measurement more than forty strain readings can be recorded and used to estimate the residual stresses over a region about 4% to 96% of the thickness.

2.0 MEASUREMENT OF RESIDUAL STRESSES THROUGH THE THICKNESS OF WELDS

Specimens containing welds H8, H10, H9, and H12 (the support leg weld) were cut out from coupons removed from the main body of the shroud and vessel structure. Since the state of residual stress changes as the specimens are cut out from the coupons, the original residual stresses σ consist of two parts

$$\sigma = \sigma_1 + \sigma_2 \tag{3}$$

in which σ_1 is the stress to be measured in a specimen and σ_2 is the change of the stress when the specimen was cut out. The first part of the stress can be obtained by the crack compliance method while the second part will be estimated by the finite element method based on the strain data recorded when the specimen is cut out from the coupon. In this report the results for the first part of the residual stresses (σ_1) are presented.

For all the specimens the region of the weld surface was found to have been subjected to machining or grinding. Therefore, the residual stresses near the surface are expected to be influenced by machining or grinding as well as welding. Because the surfaces of the as received parts were too rough for attaching strain gages directly, polishing using sand paper was carried out to smooth the surface (standard procedure recommended by strain gage supplier. This process, however, is

2

expected to have very little influence on the residual stresses in the as received specimens.

2.1 Residual Stress distribution Measured for Weld H8

Weld H8 was located between the shroud support plate (baffle plate) and core shroud. Figure 3 shows the configuration of the specimen and the finite element mesh used for numerical computations.

Content Deleted -
EPRI Proprietary Information

2.2 Residual Stress distribution Measured for Weld H10

Weld H10 joins the core shroud to the shroud support leg. Figure 6 shows the configuration of the specimen and the finite element mesh used for numerical computations.

Content Deleted -
EPRI Proprietary Information

Content Deleted -
EPRI Proprietary Information

2.3 Residual Stress distribution Measured in Shroud Support Plate for Weld H9

Weld H9 joins the shroud support plate to the vessel wall. Residual stresses were measured through the thickness of both the shroud support plate and the vessel wall.

Content Deleted -
EPRI Proprietary Information

2.4 Residual Stress distribution Measured in Vessel Wall for Weld H9

For weld H9 on the vessel wall the measurement was carried out on a plane about 5/32 inch from the toe of the weld. Figure 12 shows the configuration of the specimen and the finite element mesh used for numerical computations.

Content Deleted -
EPRI Proprietary Information

2.5 Residual Stress distribution Measured for the Shroud Support Leg Weld (H12)

The shroud support leg and the vessel wall was joined by the shroud support leg weld (H12). The configuration of the specimen, plane of measurement, and the finite element mesh used for numerical computations are shown in Fig. 15.

3.0 MEASUREMENT OF RESIDUAL STRESSES NEAR THE SURFACE OF WELD H9

In addition to the through thickness measurements, near surface stress measurements were also carried out at two locations for weld H9.

4.0 CONCLUSION

Residual stress distributions in four weld configurations were measured using the crack compliance methods. All tests were carried out by high precision numerical controlled EDWM. Strain data recorded during tests were found to be both stable and consistent. To minimize the influence of measurement error, a least squares fit was used to obtain the residual stresses from the average of the strain readings recorded by two strain gages.

Content Deleted -
EPRI Proprietary Information

5.0 REFERENCES

1. Cheng, W. and Finnie, I., "An Overview of the Crack Compliance Method for Residual Stress Measurement," Proceedings of Fourth Int. Conf. on Residual Stresses, pp.449-458, 1994.

2. Cheng, W. and Finnie, I., "A Comparison of the Strains due to Edge Cracks and Cuts of Finite Width With Applications to Residual Stress Measurement," *ASME J. of Eng. Mat. and Tech.*, 115, pp. 220-226, 1993.

3. Cheng, W., Gremaud, M. and Finnie, I., "The Compliance Method for Measurement of Near surface Residual Stresses - Analytical Background," *ASME J. of Eng. Mat. and Tech.* 116, pp. 550-555, 1994.

Table 1 Material Properties Used in Computation

Elastic modulus $E = 30 \times 10^6$ psi	Poisson's ratio $\mu = 0.3$

Table 2 Configuration and strains measured for near surface stress measurement No. 1 of weld H9

**Content Deleted -
EPRI Proprietary Information**

Table 3 Configuration and strains measured for near surface stress measurement No. 2 of weld H9

**Content Deleted -
EPRI Proprietary Information**

Content Deleted -
EPRI Proprietary Information

Figure 1 Illustration of linear superposition for determining strains due to introducing a crack into a body with residual stresses.

**Content Deleted -
EPRI Proprietary Information**

Figure 2. Residual stress distribution measured by introducing a cut of increasing depth while the change of strain is recorded by strain gages on the back face.

**Content Deleted -
EPRI Proprietary Information**

Figure 3 Finite element mesh for the specimen containing weld H8 to model a cut through the thickness of the shroud support plate.

**Content Deleted -
EPRI Proprietary Information**

Figure 4. Strain readings recorded when a cut of progressively increasing depth introduced to weld ER.

13

Content Deleted -
EPRI Proprietary Information

Figure 5. Residual radial stress distribution (σ_r) for weld H8 as a function of the distance normalized by the thickness of the shroud support plate.

**Content Deleted -
EPRI Proprietary Information**

Figure 5. Specimen configuration and finite element mesh for weld H10.

**Content Deleted -
EPRI Proprietary Information**

Figure 7. Strain readings recorded when a cut of progressively increasing depth introduced to weld H10.

**Content Deleted -
EPRI Proprietary Information**

Figure 8. Residual axial stress distribution (σ_a) for weld H10 as a function of the distance normalized by the thickness of the shroud support cylinder.

**Content Deleted -
EPRI Proprietary Information**

Figure 9. Finite element mesh for the specimen containing weld H9. The residual axial stress distribution σ_z is measured through the thickness of the shroud support plate. Also shown is the location of the near surface measurement No. 1.

**Content Deleted -
EPRI Proprietary Information**

Figure 10. Strain readings recorded when a cut of progressively increasing depth introduced to weld H9 through the thickness of the shroud support plate.

Figure 11. Residual radial stress distribution (σ_r) as a function of the distance normalized by the thickness of the shroud support plate (baffle plate) for weld H9.

Content Deleted -
EPRI Proprietary Information

Figure 12. Finite element mesh for the specimen containing weld H9. The residual axial stress distribution (σ_z) is measured through the thickness of the vessel wall. Also shown is the location of the near surface measurement No. 2.

**Content Deleted -
EPRI Proprietary Information**

Figure 13. Strain readings recorded when a cut of progressively increasing depth introduced to weld H9 through the thickness of the vessel wall.

**Content Deleted -
EPRI Proprietary Information**

Figure 14. Residual axial stress distribution (σ_z) as a function of the distance normalized by the thickness of the vessel wall for weld H9.

**Content Deleted -
EPRI Proprietary Information**

Figure 15. Finite element mesh for the specimen containing the shroud support leg weld (H12).

**Content Deleted -
EPRI Proprietary Information**

Figure 16. Strain readings recorded when a cut of progressively increasing depth introduced through the thickness of the shroud support leg weld (H12).

**Content Deleted -
EPRI Proprietary Information**

Figure 17. Residual stress distribution (normal to the plane of cut) for weld H12 as a function of the distance normalized by the thickness of the shroud support leg weld on the plane of cut.

**Content Deleted -
EPRI Proprietary Information**

Figure 18. Near surface residual stress distribution as a function of the distance measured at the location shown in Fig. 9 for weld H9.

Content Deleted -
EPRI Proprietary Information

Figure 19. Near surface residual stress distribution in the weld as a function of the distance measured at the location shown in Fig. 12 for weld H9.

APPENDIX C

CRACK GROWTH EVALUATION RESULTS

**Content Deleted -
EPRI Proprietary Information**

Figure C-1. Crack Growth Results for Weld H8 (Bottom-to-Top) – NWC

**Content Deleted -
EPRI Proprietary Information**

Figure C-2. Crack Growth Results for Weld H8 (Bottom-to-Top) – High Purity NWC

**Content Deleted -
EPRI Proprietary Information**

Figure C-3.. Crack Growth Results for Weld H8 (Bottom-to-Top) - HWC

**Content Deleted -
EPRI Proprietary Information**

Figure C-4. Crack Growth Results for Weld H8 (Top-to-Bottom) – NWC

Content Deleted -
EPRI Proprietary Information

Figure C-5. Crack Growth Results for Weld H8 (Top-to-Bottom) – High Purity NWC

**Content Deleted -
EPRI Proprietary Information**

Figure C-6. Crack Growth Results for Weld H8 (Top-to-Bottom) –HWC

**Content Deleted -
EPRI Proprietary Information**

Figure C-7. Crack Growth Results for Weld H9 (Top-to-Bottom) –NWC

**Content Deleted -
EPRI Proprietary Information**

Figure C-8. Crack Growth Results for Weld H9 (Top-to-Bottom) – High Purity NWC

**Content Deleted -
EPRI Proprietary Information**

Figure C-9. Crack Growth Results for Weld H9 (Top-to-Bottom) – HWC

**Content Deleted -
EPRI Proprietary Information**

Figure C-10. Crack Growth Results for Weld H10 – NWC

**Content Deleted -
EPRI Proprietary Information**

Figure C-11. Crack Growth Results for Weld H10 – High Purity NWC

**Content Deleted -
EPRI Proprietary Information**

Figure C-12. Crack Growth Results for Weld H10 – HWC

**Content Deleted -
EPRI Proprietary Information**

Figure C-13. Crack Growth Results for Weld H11 – NWC

**Content Deleted -
EPRI Proprietary Information**

Figure C-14. Crack Growth Results for Weld H11 – High Purity NWC

**Content Deleted -
EPRI Proprietary Information**

Figure C-15. Crack Growth Results for Weld H11 – HWC

**Content Deleted -
EPRI Proprietary Information**

Figure C-16. Crack Growth Results for Weld H12 Actual – NWC

**Content Deleted -
EPRI Proprietary Information**

Figure C-17. Crack Growth Results for Weld H12 Actual – High Purity NWC

**Content Deleted -
EPRI Proprietary Information**

Figure C-18. Crack Growth Results for Weld H12 Actual – HWC

**Analytical Prediction of Residual Stresses
in BWR Shroud Support Structure Welds**

December 1998

Prepared by:

A. P. L. Turner
J. E. Broussard
E. S. Hunt

Prepared for

Table of Contents

Analytical Prediction of Residual Stresses in Shroud Welds

The purpose of this appendix is to describe a finite element analysis (FEA) which was performed to compute residual stresses in welds of the BWR core shroud support structure design which includes support legs to the lower head of the reactor pressure vessel (RPV).

D-1 Weld Joints Analyzed

BWR core shroud support structures have a number of different designs. The design addressed in this appendix is shown in Figure D-1. The support structure consists of twelve equal size, equally spaced legs between the RPV bottom head and a shroud support cylinder. Lateral support is provided by an annular support plate (baffle plate) between the outside diameter (OD) of the shroud support cylinder and the inside diameter (ID) of the RPV. The baffle plate has holes for mounting the recirculation jet pumps. All components of the shroud support structure are made from nickel Alloy 600. The dimensions used for the model were based on the River Bend reactor, but a similar design is used in a number of plants. The calculated residual stresses are considered to be typical for all plants of similar design.

The River Bend shroud support system is twelve fold symmetric with the exception that access manways replace the jet pumps at two diametrically opposite positions.

Thus, there are ten jet pump assemblies and two manways around the circumference of the shroud support assembly. It is considered that the differences between the jet pump and manway locations are negligible in terms of the structural characteristics of the support system. Therefore, a finite element model of a 15-degree segment of the RPV and shroud support structure, as shown in Figure D-2, with mirror boundary conditions on the radial plane boundaries of the model accurately represents the complete vessel and supports.

Five welds were modeled in the finite element analysis. The weld locations are shown in Figure D-1 and are given designations as follows:

H8   Weld connecting the ID of the shroud support plate to the OD of the shroud support cylinder.

H9   Weld connecting the OD of the shroud support plate to the ID of the RPV

H10   Weld between the top of a support leg and the bottom of the shroud support cylinder.

H11   Weld between the bottom of a support leg and a pedestal attached to the lower head of the RPV when pedestals are used. The shroud support drawing indicates that pedestals are optional. No pedestals were used with the River Bend legs. Either an H11 or an H12 weld is used to attach the support leg to the lower head of the RPV.

H12   Weld directly between the bottom of a support leg and the lower head of the RPV (no pedestal used). Either an H11 or an H12 weld is used to attach the support leg to the lower head of the RPV.

Several different companies fabricated BWR reactor vessels and they used different support system designs and fabrication sequences.[1] The weld sequence used in the analysis is based on procedures used by Chicago Bridge and Iron (CBI), the fabricator of the River Bend reactor vessels.

**Content Deleted -
EPRI Proprietary Information**

---

[1]   David W. Gandy, et al., "Reactor Pressure Vessel Internals Survey," EPRI Repair Applications Center, June 12, 1989.

Content Deleted -
EPRI Proprietary Information

Although the welding sequence used in the model was specific to CBI practice, as it is understood from the drawings, calculations were also done where each weld was modeled individually.

Content Deleted -
EPRI Proprietary Information

One fabrication step that does have a significant influence on the final residual stresses is a vessel stress relief heat treatment.

Content Deleted -
EPRI Proprietary Information

Stress data from the FEA analyses were used as inputs for the crack stress intensity predictions described in the main body of this report.

D-2 Analysis Approach

Welding residual stresses in the support leg and baffle plate welds were computed using the ANSYS finite element code (Revision 5.3).

Factors Which Affect Weld Residual Stresses

The residual stresses in the vicinity of shroud support structure welds depend upon many factors including:

- Dimensions of the components and welds

- Restraints on the weld joint as it cools

- Thermal and mechanical properties of the base metal and weld metal as a function of temperature

- Thermal and physical characteristics of the welding process (e.g., heat input rate, weld rod size, number and distribution of weld passes, welding speed, interpass temperature)

- Fabrication and heat treatment history of the shroud assembly

All of these factors can have a significant impact on the final stresses existing after the last weld pass has cooled.

Key Modeling Assumptions

While all of the factors described in the previous paragraph can affect residual stresses in the parts after welding, many of these variables are difficult to quantify.

**Content Deleted -
EPRI Proprietary Information**

**Content Deleted -
EPRI Proprietary Information**

Material Properties

The welding process raises the weld metal and portions of the base metal to temperatures above the liquidus temperature (about 2460 °F for Alloy 600). In addition, portions of the base metal are heated sufficiently to affect the thermal and mechanical properties of the material. Consequently, the analyses were performed using temperature-dependent material properties. Specific values used in the

---

[1] "Evaluation of Crack Growth in BWR Stainless Steel RPV Internals," BWR Vessel and Internals Project, Topical Report TR-105873, 2nd Draft Report, November 1995. Appendix H.

analysis are reported in Table D-1. To the extent possible, properties are taken from tabulations in the ASME Boiler and Pressure Vessel Code.[1]

---

[1]   ASME Boiler and Pressure Vessel Code, Section II, Part D, 1995 Edition. American Society of Mechanical Engineers. New York, 1995.

Table D-1

Temperature-Dependent Material Properties Used in Finite Element Analysis

**Content Deleted -
EPRI Proprietary Information**

Table D-1 (cont.)

Temperature-Dependent Material Properties Used in Finite Element Analysis

**Content Deleted -
EPRI Proprietary Information**

Finite Element Mesh Characteristics

The finite element models consist of ANSYS three-dimensional SOLID70 thermal and SOLID45 structural elements. All elements are eight node solids except for isolated locations where degenerate wedge shaped elements are used. A 15-degree segment of the RPV and shroud support structure were modeled as shown in Figure D-2. Refined meshes were used in the vicinities of the welds where temperature and stress gradients are high as shown in Figure D-3 and results figures. Larger elements were used for the remainder of the model.

Fabrication Sequence

Four welds were initially modeled sequentially in the FEA.

Content Deleted -
EPRI Proprietary Information

Modeling of Welding Process

Each weld pass is analyzed by a two step process consisting of a thermal analysis to determine the temperature distributions as a function of time and a structural analysis to determine the resultant stresses.

Content Deleted -
EPRI Proprietary Information

Thermal Model. The thermal analysis involves application of thermal boundary conditions followed by simulation of each welding pass.

Content Deleted -
EPRI Proprietary Information

**Content Deleted -
EPRI Proprietary Information**

<u>Structural Model</u>. After calculating the temperature distributions for the welding passes, the element and nodal geometry was converted to a structural model by changing the SOLID70 thermal elements to SOLID45 structural elements. The following structural boundary conditions were used:

**Content Deleted -
EPRI Proprietary Information**

**Content Deleted -
EPRI Proprietary Information**

Modeling of Post Weld Heat Treatment

Some BWR pressure vessel fabricators performed a stress relief heat treatment at 1150 °F on the RPV after the shroud support structure had been installed. The purpose of the heat treatment was for post weld stress relief of the pressure vessel welds, but it also had an effect on the residual stresses in the support structure.

**Content Deleted -
EPRI Proprietary Information**

Content Deleted -
EPRI Proprietary Information

Content Deleted -
EPRI Proprietary Information

Effects of Stress Relief Post Weld Heat Treatment

Content Deleted -
EPRI Proprietary Information

Table D-2

Peak Residual Stresses

Content Deleted -
EPRI Proprietary Information

**Content Deleted -
EPRI Proprietary Information**

D-4 Comparison of Calculated and Measured Residual Stresses

As part of a separate effort, experimental procedures were used to measure the residual stresses in the H8, H9, H10, and H12 welds, using samples of these welds cut from the duplicate River Bend shroud. No stresses could be obtained for the H11 weld geometry because this geometry did not exist for the duplicate shroud. The procedures used and the results obtained are detailed in Reference 8. A brief comparison of the calculated and measured residual stresses is included in this section; a more detailed discussion is included elsewhere in the report.

**Content Deleted -
EPRI Proprietary Information**

D-5 Use of FEA Results in Predicting Crack Stress Intensities

The results from the finite element analyses described in this appendix were used as inputs to models predicting crack stress intensities for the different welds.

FEA Work Supporting H8 and H9 Weld Crack Predictive Models

Content Deleted -
EPRI Proprietary Information

FEA Work Supporting H10 and H12 Weld Crack Predictive Models

Content Deleted -
EPRI Proprietary Information

Content Deleted -
EPRI Proprietary Information

D-6 References

1. ANSYS Finite Element Program, Revision 5.3, Swanson Analysis Systems, Inc.

2. David W. Gandy, et al., "Reactor Pressure Vessel Internals Survey," EPRI Repair Applications Center, June 12, 1989.

3. David W. Gandy, et al., "Reactor Pressure Vessel Internals Survey," EPRI Repair Applications Center, June 12, 1989.

4. "Evaluation of Crack Growth in BWR Stainless Steel RPV Internals," BWR Vessel and Internals Project, Topical ReportTR-105873, 2nd Draft Report, November 1995, Appendix H.

5. ASME Boiler and Pressure Vessel Code, Section II, Part D, 1995 Edition, American Society of Mechanical Engineers, New York, 1995.

6. "Analysis Guidelines for Backfill Modification of RPV Water Level Instrumentation," General Electric Company Report No. GENE-637-019-893, Rev. 0, August 1993.

7. "Shielded Metal Arc Welding of ASME P43 Material with GTA Pick Ups," CBI Nuclear Company, Welding Procedure, WTS 309-2, P-43, 10/7/68, Rev. 5 1/7/75.

8. Weili Cheng, et al., "Measurements of Residual Stresses in BWR Core Shroud Support Welds,"

Content Deleted -
EPRI Proprietary Information

Figure D-1. Reactor Vessel and Shroud Support Model

Content Deleted -
EPRI Proprietary Information

Figure D-2 Model Weld Geometry

Content Deleted -
EPRI Proprietary Information

Figure D-3a. Weld 18 Weld Sequence and Approximate Mesh

Content Deleted -
EPRI Proprietary Information

Figure D-3b. Weld 119 Weld Sequence and Approximate Mesh

Content Deleted -
EPRI Proprietary Information

Figure D-3c. Weld H10 Weld Sequence and Approximate Mesh

Content Deleted -
EPRI Proprietary Information

Figure D-3d. Weld H11 Weld Sequence and Approximate Mesh

**Content Deleted -
EPRI Proprietary Information**

Figure D-3e. Weld H12 Weld Sequence and Approximate Mesh

**Content Deleted -
EPRI Proprietary Information**

Figure D-4

Weld H8 After Welding
Radial Stress (SX)

**Content Deleted -
EPRI Proprietary Information**

Figure D-5

Weld H8 After Welding
Circumferential Stress (SY)

**Content Deleted -
EPRI Proprietary Information**

<u>Figure D-6</u>

Weld H9 After Welding
Radial Stress (SX)

**Content Deleted -
EPRI Proprietary Information**

<u>Figure D-7</u>

Weld H9 After Welding
Circumferential Stress (SY)

**Content Deleted -
EPRI Proprietary Information**

<u>Figure D-8</u>

Weld H10 After Welding
Vertical Stress (SZ)

**Content Deleted -
EPRI Proprietary Information**

<u>Figure D-9</u>

Weld H10 After Welding
Circumferential Stress (SY)

**Content Deleted -
EPRI Proprietary Information**

Figure D-10

Weld H11 After Welding
Vertical Stress (SZ)

**Content Deleted -
EPRI Proprietary Information**

Figure D-11

Weld H11 After Welding
Circumferential Stress (SY)

**Content Deleted -
EPRI Proprietary Information**

Figure D-12

Weld H12 After Welding
Perpendicular Stress (SZ)

**Content Deleted -
EPRI Proprietary Information**

Figure D-13

Weld H12 After Welding
Circumferential Stress (SY)

**Content Deleted -
EPRI Proprietary Information**

<u>Figure D-14a</u>

Weld H10 After Welding
Upper HAZ (from above)
Vertical Stress (SZ)

**Content Deleted -
EPRI Proprietary Information**

<u>Figure D-14b</u>

Weld H10 After Welding
Lower HAZ (from below)
Vertical Stress (SZ)

**Content Deleted -
EPRI Proprietary Information**

Figure D-15a

Weld H11 After Welding
Upper HAZ (from above)
Vertical Stress (SZ)

**Content Deleted -
EPRI Proprietary Information**

Figure D-15b

Weld H10 After Welding
Lower HAZ (from below)
Vertical Stress (SZ)

**Content Deleted -
EPRI Proprietary Information**

Figure D-16a

Weld H12 After Welding
Upper HAZ (from above)
Perpendicular Stress (SZ)

**Content Deleted -
EPRI Proprietary Information**

Figure D-16b

Weld H12 After Welding
Lower HAZ (from below)
Perpendicular Stress (SZ)

**Content Deleted -
EPRI Proprietary Information**

<u>Figure D-17</u>

Weld H8 After PWHT
Radial Stress (SX)

**Content Deleted -
EPRI Proprietary Information**

<u>Figure D-18</u>

Weld H8 After PWHT
Circumferential Stress (SY)

**Content Deleted -
EPRI Proprietary Information**

Figure D-19

Weld H9 After PWHT
Radial Stress (SX)

**Content Deleted -
EPRI Proprietary Information**

Figure D-20

Weld H9 After PWHT
Circumferential Stress (SY)

**Content Deleted -
EPRI Proprietary Information**

Figure D-21

Weld H10 After PWHT
Vertical Stress (SZ)

**Content Deleted -
EPRI Proprietary Information**

Figure D-22

Weld H10 After PWHT
Circumferential Stress (SY)

**Content Deleted -
EPRI Proprietary Information**

Figure D-23

Weld H11 After PWHT
Vertical Stress (SZ)

**Content Deleted -
EPRI Proprietary Information**

Figure D-24

Weld H11 After PWHT
Circumferential Stress (SY)

**Content Deleted -
EPRI Proprietary Information**

Figure D-25

Weld H12 After PWHT
Perpendicular Stress (SZ)

**Content Deleted -
EPRI Proprietary Information**

Figure D-26

Weld H12 After PWHT
Circumferential Stress (SY)

**Content Deleted -
EPRI Proprietary Information**

Figure D-27a. H8 Support Cylinder HAZ After Welding - Leg Centerline

**Content Deleted -
EPRI Proprietary Information**

Figure D-27b. H8 Support Cylinder HAZ After Stress Relief - Leg Centerline

**Content Deleted -
EPRI Proprietary Information**

Figure D-28a. H8 Support Plate HAZ After Welding - Leg Centerline

**Content Deleted -
EPRI Proprietary Information**

Figure D-28b. H8 Support Plate HAZ After Stress Relief - Leg Centerline

Figure D-29a. H8 Weld Centerline After Welding - Leg Centerline

Figure D-29b. H8 Weld Centerline After Stress Relief - Leg Centerline

Figure D-30a. H9 Reactor Vessel HAZ After Welding - Leg Centerline

Figure D-30b. H9 Reactor Vessel HAZ After Stress Relief - Leg Centerline

Content Deleted -
EPRI Proprietary Information

Figure D-31a. H9 Support Plate HAZ After Welding - Leg Centerline

Content Deleted -
EPRI Proprietary Information

Figure D-31b. H9 Support Plate HAZ After Stress Relief - Leg Centerline

Content Deleted -
EPRI Proprietary Information

Figure D-32a. H9 Weld Centerline After Welding - Leg Centerline

Content Deleted -
EPRI Proprietary Information

Figure D-32b. H9 Weld Centerline After Stress Relief - Leg Centerline

Content Deleted -
EPRI Proprietary Information

Figure D-33a. H10 Upper HAZ After Welding - Leg Centerline

Content Deleted -
EPRI Proprietary Information

Figure D-33b. H10 Upper HAZ After Stress Relief - Leg Centerline

Figure D-34a. H10 Lower HAZ After Welding - Leg Centerline

Figure D-34b. H10 Upper HAZ After Stress Relief - Leg Centerline

Figure D-35a. H10 Weld Centerline After Welding - Leg Centerline

Figure D-35b. H10 Weld Centerline After Stress Relief - Leg Centerline

Figure D-36a. H11 Upper HAZ After Welding - Leg Centerline

Figure D-36b. H11 Upper HAZ After Stress Relief - Leg Centerline

Content Deleted -
EPRI Proprietary Information

Figure D-37a. H11 Lower HAZ After Welding - Leg Centerline

Content Deleted -
EPRI Proprietary Information

Figure D-37b. H11 Lower HAZ After Stress Relief - Leg Centerline

**Content Deleted -
EPRI Proprietary Information**

Figure D-38a. H11 Weld Centerline After Welding - Leg Centerline

**Content Deleted -
EPRI Proprietary Information**

Figure D-38b. H11 Weld Centerline After Stress Relief - Leg Centerline

Content Deleted -
EPRI Proprietary Information

Figure D-39a. H12 Upper HAZ After Welding - Leg Centerline

Content Deleted -
EPRI Proprietary Information

Figure D-39b. H12 Upper HAZ After Stress Relief - Leg Centerline

**Content Deleted -
EPRI Proprietary Information**

Figure D-40a. H12 Lower HAZ After Welding - Leg Centerline

**Content Deleted -
EPRI Proprietary Information**

Figure D-40b. H12 Lower HAZ After Stress Relief - Leg Centerline

Content Deleted -
EPRI Proprietary Information

Figure D-41a. H12 Weld Centerline After Welding - Leg Centerline

Content Deleted -
EPRI Proprietary Information

Figure D-41b. H12 Weld Centerline After Stress Relief - Leg Centerline

**Content Deleted -
EPRI Proprietary Information**

Figure D-42. H8 Cut Line Residual Stresses Perpindicular to Cut Line

Content Deleted -
EPRI Proprietary Information

Figure D-43. I19 Cut Line Residual Stresses Perpindicular to Cut Line

Content Deleted -
EPRI Proprietary Information

Figure D-44. HID Cut Line Residual Stresses Perpendicular to Cut Line - Large Weld Cap on Backgouge

Content Deleted -
EPRI Proprietary Information

Figure D-45. H12 Cut Line Residual Stresses Perpindicular to Cut Line - After Removal of Bottom Weld

Content Deleted -
EPRI Proprietary Information

Figure D-46. Residual Stress Through RPV Wall Below H9 Weld

Content Deleted -
EPRI Proprietary Information

Figure D-47. Weld 118 Residual Stress (Sx) - Stresses on Cut Line - Crack Propagating from Bottom to Top

Content Deleted -
EPRI Proprietary Information

Figure D-48. Weld 119 with PWHT Residual Stress (Sx) - Stresses on Cut Line - Crack Propagating
from Top to Bottom

Target:

Nuclear Power

About EPRI

EPRI creates science and technology solutions for the global energy and energy services industry. U.S. electric utilities established the Electric Power Research Institute in 1973 as a nonprofit research consortium for the benefit of utility members, their customers, and society. Now known simply as EPRI, the company provides a wide range of innovative products and services to more than 1000 energy-related organizations in 40 countries. EPRI's multidisciplinary team of scientists and engineers draws on a worldwide network of technical and business expertise to help solve today's toughest energy and environmental problems.

EPRI. Powering Progress

TR-108710